Ca^{2+}-Triggered (de)ubiquitination Events in Synapses

Authors
Sofia Ainatzi, Svenja V. Kaufmann, Ivan Silbern, Svilen V. Georgiev, Sonja Lorenz, Silvio O. Rizzoli, and Henning Urlaub

Correspondence
hurlaub@gwdg.de

In Brief
Neuronal communication relies on neurotransmitter release from synaptic vesicles (SVs). However, little is known about ubiquitination in this process. To address this, we analyzed resting and stimulated synaptosomes (isolated synapses) by quantitative mass spectrometry. We identified more than 5000 ubiquitination sites, with the most pronounced changes in CaMKIIα and the clathrin adaptor protein AP180. K291 ubiquitination influences CaMKIIα activity and synaptic function. We suggest that ubiquitination in response to synaptic activity is an important regulator of synaptic function.

Graphical Abstract

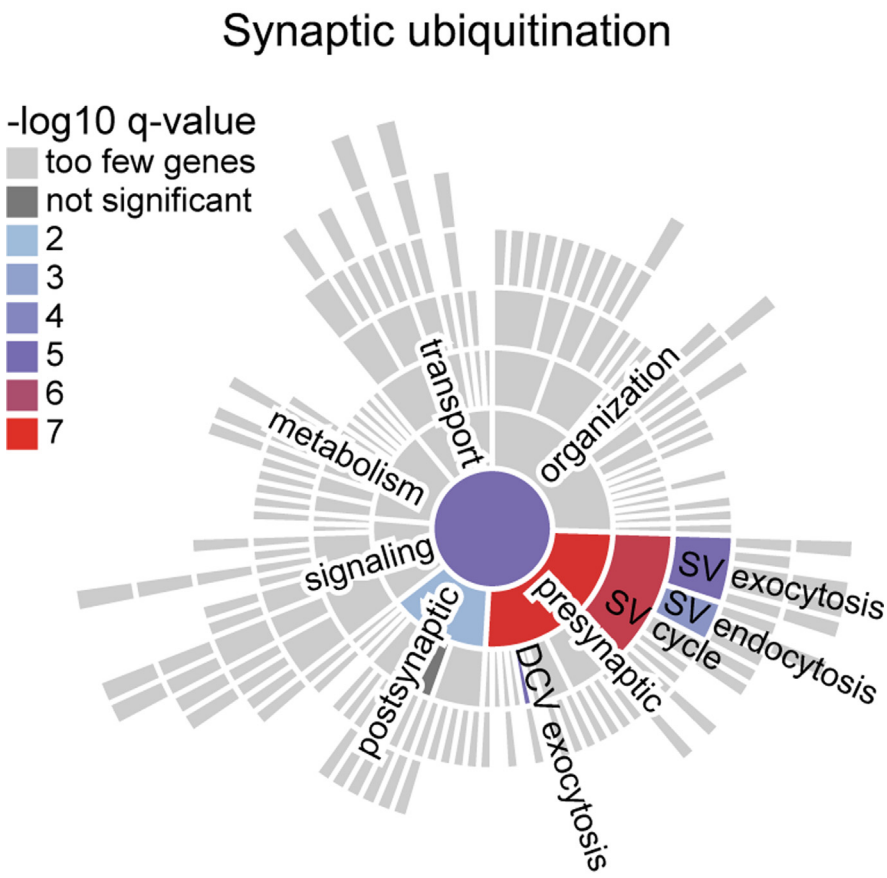

Highlights

- We identified more than 5000 ubiquitination sites on ~2000 proteins in synapses.
- Several proteins showed significant changes in ubiquitination in response to Ca^{2+} influx.
- CaMKIIα and the clathrin adaptor protein AP180 change profoundly.
- K291 ubiquitination influences CaMKIIα activity and synaptic function.

2025, Mol Cell Proteomics *24(4)*, 100946

https://doi.org/10.1016/j.mcpro.2025.100946

Ca^{2+}-Triggered (de)ubiquitination Events in Synapses

Sofia Ainatzi[1,2], Svenja V. Kaufmann[1,2], Ivan Silbern[1,2], Svilen V. Georgiev[3], Sonja Lorenz[4], Silvio O. Rizzoli[3], and Henning Urlaub[1,2,5,6,*]

Neuronal communication relies on neurotransmitter release from synaptic vesicles (SVs), whose dynamics are controlled by Ca^{2+}-dependent pathways, as many thoroughly studied phosphorylation cascades. However, little is known about other post-translational modifications, such as ubiquitination. To address this, we analyzed resting and stimulated synaptosomes (isolated synapses) by quantitative mass spectrometry. We identified more than 5000 ubiquitination sites on ~2000 proteins, the majority of which participate in SV recycling processes. Several proteins showed significant changes in ubiquitination in response to Ca^{2+} influx, with the most pronounced changes in CaMKIIα and the clathrin adaptor protein AP180. To validate this finding, we generated a CaMKIIα mutant lacking the ubiquitination target site (K291) and analyzed it both in neurons and non-neuronal cells. K291 ubiquitination, close to an important site for CaMKIIα autophosphorylation (T286), influences the synaptic function of this kinase. We suggest that ubiquitination in response to synaptic activity is an important regulator of synaptic function.

In a chemical synapse, information flows from a presynaptic neuron to a postsynaptic cell through the Ca^{2+}-regulated release of neurotransmitters (NTs). NTs are stored in synaptic vesicles (SVs) located within the presynaptic nerve terminal. Functionally distinct pools of SVs co-exist within the presynaptic bouton, with only a small fraction actively participating in SV trafficking during low-frequency stimulation (1). Specifically, SVs that are docked at specialized release sites, known as the active zone (AZ), are primed for SV exocytosis/fusion. The SV docking and priming at the AZ is mediated by a large protein complex consisting of scaffolding proteins (RIM, Munc13, RIM-BP, liprins, ELKS, bassoon, and piccolo) (2). Primed SVs at the AZ are the first to fuse with the presynaptic plasma membrane in response to stimulation, forming the readily releasable pool (RRP) (1). Exocytotic fusion of SVs is mediated by the SNAREs (3) and regulated by the Ca^{2+}-sensing protein synaptotagmin (4) and other proteins, such as Munc18 (5) and complexins (4). After SV exocytosis, SV membranes are endocytosed primarily by clathrin-mediated endocytosis (CME) (6) and SVs are regenerated to participate in another round of NT release.

Post-translational modifications (PTMs), such as protein phosphorylation, serve as a molecular mechanism for fine-tuning the SV cycle. Arguably, the best-characterized example of such modulation is the regulation of SV mobility and availability for exocytosis by a conserved family of phosphoproteins, the synapsins (7, 8). Synapsins are SV-associated proteins that link SVs together to form a cluster of SVs, the reserve pool (RP) (1, 9). Several presynaptic kinases, including Ca^{2+}/calmodulin-dependent kinase II (CaMKII), regulate the phosphorylation state of synapsins (9). CaMKII-dependent phosphorylation of synapsin at specific sites (S566, S603) during stimulation reduces binding to actin and SVs, thereby releasing the SVs from the RP and making them available for exocytosis (9). In contrast to synapsins, several proteins involved in CME, termed dephosphins (10), are dephosphorylated during stimulation to facilitate SV endocytosis, such as the adaptor proteins epsin, eps15 and AP180 (10, 11). In addition to these proteins, recent mass spectrometry (MS)-based phosphoproteomic studies revealed that a large number of presynaptic proteins undergo phosphorylation changes in response to Ca^{2+} influx, suggesting that phosphorylation is a driver of the changes in protein–protein interactions that occur in the synapse during stimulation (11–13).

In addition to phosphorylation, a growing body of studies indicates that another PTM, protein ubiquitination, plays an important role at the synapse. In general, K48-linked ubiquitin chains target substrate proteins for degradation by the 26S proteasome (14), thereby regulating protein quality control as well as diverse other cellular functions (15), whereas mono-ubiquitination and other ubiquitin linkage types are often

From the [1]Bioanalytical Mass Spectrometry, Max Planck Institute for Multidisciplinary Sciences, Goettingen, Germany; [2]Bioanalytics, Institute of Clinical Chemistry, and [3]Department of Neuro- and Sensory Physiology, University Medical Center, Goettingen, Germany; [4]Ubiquitin Signaling Specificity, Max Planck Institute for Multidisciplinary Sciences, Goettingen, Germany; [5]Cluster of Excellence Multiscale Bioimaging: from Molecular Machines to Networks of Excitable Cells (MBExC), University of Göttingen, Germany; [6]Göttingen Center for Molecular Biosciences, Georg August University Göttingen, Germany

*For correspondence: Henning Urlaub, hurlaub@gwdg.de.

https://doi.org/10.1016/j.mcpro.2025.100946

associated with non-degradative processes, such as membrane protein trafficking, DNA repair, signaling pathways, and the activation of protein kinases (14). Multiple mono-ubiquitination and K-63 linkages have been implicated in the multivesicular endosomal sorting of plasma membrane proteins followed by their degradation in lysosomes (16). Ubiquitination typically occurs at the primary amino group of Lys residues of substrates, mediated by the sequential action of three enzymes (ubiquitin-activating enzyme (E1), ubiquitin-conjugating enzyme (E2), and ubiquitin ligase (E3) enzymes), and its removal is achieved by deubiquitinating enzymes (DUBs) (14).

Indeed, synaptic proteins undergo ubiquitination and degradation by the proteasome (UPS) (17–21), including a number of AZ proteins, such as RIM and Munc13 (20–23). Spatiotemporal regulation of ubiquitination and degradation is achieved at the presynaptic nerve terminals through the AZ scaffold proteins bassoon and piccolo (24). Lastly, perturbation of the UPS *via* pharmacological agents was shown to influence NT release in different preparations (20, 25). Apart from the degradative roles of ubiquitin, ubiquitin also has non-degradative roles in the presynapse. One element suggesting a modulatory role of ubiquitination is the high rate at which protein ubiquitination occurs and its correlation with synaptic activity. Specifically, a rapid decrease in the total ubiquitination levels was observed upon Ca^{2+} influx in isolated nerve terminals, an effect that was only partially reversed by proteasome inhibition (26). The same study showed that the clathrin-adaptor proteins, epsin-1 and eps15, underwent fast deubiquitination in response to depolarization-triggered Ca^{2+} influx (26). Finally, acute pharmacological inhibition of protein ubiquitination in cultured neurons was shown to elicit a rapid increase in spontaneous neurotransmitter release (25).

However, it is not known which synaptic proteins are ubiquitinated at which sites and whether their ubiquitination status changes in different states of the synapse. Here, liquid chromatography-tandem mass spectrometry (LC-MS/MS) offers the possibility of comprehensive identification and relative quantification of ubiquitination sites on proteins. Based on improved immunoaffinity purification strategies of ubiquitinated peptides (27, 28), it has become evident that ubiquitination is a very prominent protein modification in cells, and importantly, that changes in the ubiquitination state of proteins are observed under different conditions in various cellular systems (15, 28–33). To date, only a few studies have characterized protein ubiquitination in brain tissue by MS, but no ubiquitinome analyses have been performed in isolated nerve terminals (34, 35). Particularly in this context, it remains to be determined which synaptic proteins undergo ubiquitination changes in response to Ca^{2+} influx, illuminating the non-degradative functions of ubiquitination in synapses. In this study, we performed a proteome-wide quantification analysis of ubiquitinated proteins in isolated nerve terminals, termed “synaptosomes” (36). Synaptosomes are considered a valid model system of the synapse, as they contain SVs, mitochondria and the molecular machinery required for the SV cycle (36, 37). We isolated synaptosomes from rat brains and subjected them to a bottom-up proteomic workflow incorporating antibody-based enrichment of formerly ubiquitinated peptides, followed by labeling with isobaric tandem mass tag (TMT) reagents and LC-MS/MS analysis (28, 38). Our analysis identified 41 proteins that undergo significant ubiquitination changes in response to Ca^{2+} and provides the first synapse-specific inventory of ubiquitination sites. Prominent changes in ubiquitination are observed for Ca^{2+}/calmodulin-dependent kinase II alpha (CaMKIIα) and the clathrin adaptor protein 180 (AP180) upon depolarization. Lastly, we have functionally characterized one of these newly discovered ubiquitination sites, K291 of CaMKIIα.

EXPERIMENTAL PROCEDURES

Materials

LC/MS-grade water, acetonitrile (ACN), methanol, chloroform, $CaCl_2$, KCl, KH_2PO_4, $MgCl_2$, NaCl, $NaHCO_3$, $NaHPO_4$, 25% (v/v) NH_4OH, sucrose and glucose were purchased from Merck, Darmstadt, Germany. Triethylammonium bicarbonate (TEAB), EGTA, PM400-Ficoll, NADP, L-glutamic dehydrogenase from bovine liver (GluDH), formic acid (FA), glycolic acid (GA), guanidine hydrochloride, tris(2-carboxylethyl)phosphine (TCEP), chloroacetamide (CAA), PR-619 were purchased from Sigma-Aldrich, Taufkirchen, Germany. HEPES was obtained from VWR Chemicals, Darmstadt, Germany. Trifluoracetic acid (TFA) was purchased from Roth, Karlsruhe, Germany. MS-grade trypsin and LysC were purchased from Promega. RapiGest was purchased from Waters, Milford. Pierce 660 nm protein assay, Halt Protease and phosphatase inhibitor cocktail, and isobaric TMT6plex reagents (TMT6) were obtained from Thermo Fisher Scientific.

Ethical Statement

For the primary cultures, rats (*Rattus norvegicus*, wild type, Wistar) were handled according to the specifications of the University of Göttingen and of the local authority, the State of Lower Saxony (Landesamt für Verbraucherschutz, LAVES, Braunschweig, Germany). All experiments and procedures were approved by the local authority, the Lower Saxony State Office for Consumer Protection and Food Safety (Niedersächsisches Landesamt für Verbraucherschutz und Lebensmittelsicherheit). All methods are reported in accordance with ARRIVE guidelines and were carried out in accordance with relevant guidelines and regulations. The experimental procedure was approved by the relevant institutional entity, the Tierschutzbüro of the University Medical Center Göttingen (approval number T 09/08).

For the synaptosome preparations, all procedures with rats (*R. norvegicus*, wild-type, Wistar) were conducted in the animal facility at the Max-Planck-Institute for Multidisciplinary Sciences, Göttingen. According to the German Animal Welfare Law, killing is not an experiment on animals. All requirements of § 4 TierSchG together with § 2 Satz 2, Anlage 1, Abschnitt 2, and Anlage 2 TierSchVersV were implemented.

The facility is conducted under all aspects of animal welfare. The facility is headed by a veterinarian with special education in laboratory animal science as well as gene technology and molecular genetics. Only professionally educated animal technicians are in charge of animal husbandry and care. The facility is registered according to §11

Abs. 1 TierSchG (Tierschutzgesetz der Bundesrepublik Deutschland, Animal Welfare Law of the Federal Republic of Germany) as documented by 33.23 to 42508-066-§11, dated Nov 16th, 2023 ("Erlaubnis, zum Halten von Wirbeltieren zur Versuchszwecken", "Permission to keep vertebrates for experimental purposes") by the Niedersächsisches Landesamt für Verbraucherschutz und Lebensmittelsicherheit (Lower Saxony State Office for Consumer Protection and Food Safety). According to the Animal Welfare Law of the Federal Republic of Germany (TierSchG) and the Regulation about animals used in experiments, dated 20th Dec 2022 (TierSchVersV) an animal welfare officer (specialized veterinarian in laboratory animal science) and an animal welfare committee for the institute is established.

Synaptosome Preparation and Glutamate Release Assay

Wistar rats aged between 5 and 7 weeks were sacrificed by cervical dislocation before decapitation. Whole brains were rapidly removed from the skull and cooled in ice-cold homogenization buffer (320 mM sucrose, 5 mM HEPES, pH 7.4). Cerebral cortices and cerebella were subsequently dissected and homogenized at 900 rpm using nine strokes with a Teflon/glass homogenizer. The resulting homogenate was used for the isolation of synaptosomes by the discontinuous Ficoll gradient centrifugation method, according to previously reported procedures (39). Specifically, the homogenate was centrifuged at 2988*g* for 2 min and the resulting supernatant (S1) was subjected to an additional centrifugation step at 14,462*g* for 12 min using an SS-34 fixed-angle rotor (Thermo Fisher Scientific). The crude synaptosomal pellet (P2) was resuspended in ice-cold homogenization buffer and layered onto a discontinuous Ficoll density gradient (6%/9%/13% w/v Ficoll in homogenization buffer) followed by centrifugation at 86,575*g* for 40 min using an SW-41 swinging bucket rotor (Beckman Coulter, Krefeld, Germany). The synaptosome-enriched fraction at the interphase between 9% and 13% w/v Ficoll was obtained and washed with homogenization buffer. Synaptosomes were concentrated in a final centrifugation step at 14,462*g* for 12 min using an SS-34 fixed-angle rotor (Thermo Fisher Scientific) and the resulting synaptosomal pellet was resuspended in an ice-cold homogenization buffer. Protein concentration was determined by the Pierce 660 nm protein assay following the manufacturer's instructions.

The viability of synaptosomes was assessed by using the continuous fluorometric assay of glutamate release as previously described (40). Briefly, 2 to 2.5 mg of synaptosomal protein was centrifuged at 6900*g* for 3 min in a bench-top centrifuge and resuspended in 2 ml of physiological buffer (10 mM glucose, 5 mM KCl, 140 mM NaCl, 5 mM $NaHCO_3$, 1 mM $MgCl_2$, 1.2 mM $NaHPO_4$, 20 mM HEPES, pH7.4). Synaptosomes were incubated in a physiological buffer at 37 °C for 5 min to re-establish ATP levels, followed by the addition of 1 mM NADP and either 1.3 mM $CaCl_2$ or 0.5 mM EGTA. Subsequently, the synaptosomal suspension was transferred to a quartz glass cuvette (Hellma), and the incubation at 37 °C was continued with stirring for three more minutes. 200 u of glutamate dehydrogenase was further added to the synaptosomal suspension and the NADPH-fluorescence at 440 nm was measured for 3 min in a Fluorolog-3 fluorimeter (Horiba Jobin Yvon). 50 mM KCl was then added to the synaptosomal suspension to induce glutamate release, and the NADPH fluorescence was measured for a further 1 min. Finally, the synaptosomal suspension was centrifuged at 6900*g* for 15 s in a bench-top centrifuge and the synaptosome pellet was lysed in 0.2 ml lysis buffer (6 M guanidine hydrochloride, 50 mM HEPES, pH 8, 10 mM TCEP, 40 mM CAA, 5 mM EDTA, 50 μM PR-619, 1× Halt protease and phosphatase inhibitor cocktail). For Ca^{2+}-EGTA treated synaptosomes, after the 2-minute depolarization in the presence of Ca^{2+}, EGTA was added to the suspension to a final concentration of 2 mM and NADPH-fluorescence was measured for another 2 min. Synaptosomes were then lysed and collected as described above.

Protein Precipitation and Digestion

Lysed synaptosomes were incubated at 50 °C for 30 min in the presence of 10 mM TCEP/40 mM CAA to reduce disulfide bonds and carbamidomethylate cysteine residues, respectively. Samples were briefly cooled on ice and further sonicated for 10 min using 30 s on/30 s off iterations at maximum intensity in a Bioruptor ultrasonication device (Diagenode, Seraing, Belgium). Proteins were precipitated by the methanol/chloroform precipitation method (41): Briefly, 4 and 1 sample volumes of ice-cold methanol and chloroform, respectively, were added to lysed synaptosomes, followed by the addition of 3× sample volume of water for phase separation. The samples were vortexed and subsequently centrifuged at 9000*g* for 1 min at 4 °C. The upper phase was carefully discarded, and the aggregated proteins were washed with 1 ml of ice-cold methanol. Samples were vortexed and the proteins were precipitated by centrifugation at 16,000*g* for 10 min at 4 °C. The resulting protein pellet was resuspended in a digestion buffer (0.1% RapiGest, 100 mM TEAB, pH 8) and sonicated for 10 min with 30 s on/30 s off iteration as described above. Proteins were pre-digested for 2 h at 37 °C with LysC at a protease-to-protein ratio of 1:300 (w/w). Finally, trypsin was added at a 1:90 (w/w) trypsin-to-protein ratio and the incubation was continued at 25 °C for 16 h. The next day, RapiGest was precipitated by acidifying the solution with 1% TFA and 1 h incubation at 37 °C. Peptide solutions were cleared in a bench-top centrifuge at maximum speed for 10 min and dried in a centrifugal Savant SpeedVac (Thermo Fisher Scientific). Finally, peptides were subjected to desalting using 50-mg Sep-Pak C18 Vac cartridges (Waters) according to the manufacturer's instructions. An aliquot of the desalted peptides was taken for the proteome analysis and the desalted peptides were dried in a centrifugal Savant SpeedVac (Thermo Fisher Scientific).

K-ε-GG Peptide Enrichment and TMT Labelling

K-ε-GG peptide enrichment was performed using a K-ε-GG-specific antibody (PTM-Scan ubiquitin remnant motif K-ε-GG kit, Cell Signaling Technology, Kit#5562) chemically crosslinked to agarose beads as previously described (42). Briefly, 2 to 2.5 mg of dried peptides were dissolved in 1 ml of ice-cold IAP buffer (50 mM MOPS, pH 7.2, 50 mM NaCl, 10 mM Na_3PO_4) and sonicated in the Bioruptor for 10 min using a 30 s on/30 s off cycle. Peptide solutions were cleared by centrifugation in a bench-top centrifuge at maximum speed for 3 min at 4 °C. Cleared peptide solutions were incubated with 31.25 μg of K-ε-GG-specific antibody for 2 h at 4 °C with gentle end-over-end rotation. Ab-bead conjugates were then centrifuged at 2000 *g* for 1 min and the unbound fraction was carefully removed. Ab-bead conjugates were washed 3 times with ice-cold IAP buffer followed by two washes with 100 mM HEPES, pH 8. Thereafter, beads were centrifuged at 2000 *g* for 1 min and resuspended in 200 μl HEPES, pH 8. Chemical labeling of K-ε-GG peptides still bound to the antibody was performed by adding 400 μg of TMT6 isobaric reagents to each sample and incubating for 10 min at 25 °C with shaking at 1000 rpm (32). TMT labeling was then quenched with 0.025% (v/v) hydroxylamine for 5 min at 25 °C. After quenching, Ab-beads conjugates were washed twice with 1× PBS buffer. Finally, K-ε-GG peptides were eluted by the addition of 100 μl of 0.15% (v/v) TFA and incubated for 10 min at 25 °C followed by two repetitions of the addition and incubation steps. The resulting (K-ε-GG) peptides were cleaned using C18 spin columns (Harvard Apparatus) and dried in a centrifugal Savant SpeedVac (Thermo Fisher Scientific).

K-ε-GG Peptide Enrichment for PRM Analysis

For all targeted MS analysis (PRM), protein precipitation and digestion were carried out as described above (see section 4.3) with the following exceptions. 2 mg of synaptosomal proteins were precipitated using the methanol/chloroform precipitation method and subsequently digested with LysC and trypsin using a protease-to-protein ratio (w/w) of 1:200 and 1:50, respectively. K-ε-GG peptide enrichment was performed using the K-ε-GG-specific antibody (PTMScan HS Ubiquitin/SUMO remnant motif K-ε-GG kit, Cell Signaling Technology, Kit#59322) covalently linked to magnetic beads. For the validation of several sites, 200 fmol of standard synthetic SpikeTideL K-ε-GG peptides (JPT Peptide Technologies) were added to the endogenous peptide mixture before K-ε-GG peptide enrichment. For absolute quantification, the peptide mixture was divided into two equal aliquots of 1 mg each. To each aliquot, 350 fmol of high-purity (>97%) AQUA QuantPro peptides (Thermo Fisher Scientific) were added prior to K-ε-GG peptide enrichment. Briefly, dried peptides were dissolved in 1 ml of ice-cold IAP Bind buffer and sonicated in a water bath for 2 min. Peptide solutions were cleared by centrifugation in a bench-top centrifuge at maximum speed for 5 min at 4 °C. Peptide solutions were then incubated with 7 µl of K-ε-GG-specific antibody for 3 h at 4 °c with gentle end-over-end rotation. Ab-bead conjugates were then centrifuged at 2000*g* for 5 s and the unbound fraction was carefully removed on a magnetic rack. Ab-bead conjugates were washed three times with ice-cold Wash Buffer followed by two washes with LC-MS grade water. Finally, K-ε-GG peptides were eluted by the addition of 200 µl of 0.15% (v/v) TFA, 10% can, and incubation for 15 min at 25 °C. The resulting K-ε-GG peptide solutions were dried in a centrifugal Savant SpeedVac prior to LC-MS/MS analysis. For the phosphatase treatment, dried K-ε-GG peptides were resuspended in 20 µl of 1× CutSmart buffer (New England Biolabs, B7204S) and incubated with 2.5 u of QuickCIP phosphatase (New England Biolabs, M0525L) at 37 °C for 1 h. After that, QuickCIP was heat-inactivated at 80 °C for 2 min, and the peptide solutions were desalted using C18 StageTips (Empore C18 SPE Disks, Sigma Aldrich). Briefly, StageTips were conditioned by 100 µl of 100% MeCN followed by 100 µl of 80% ACN/0.1% TFA and by 3 × 100 µl 2%ACN/0.1%TFA. Peptides were then loaded on StageTips, washed 3× with 100 ul of 2%ACN/0.1% TFA, and eluted 2× with 50 µl of 50% ACN/0.1%TFA. Eluted peptides were dried using vacuum centrifugation prior to MS analysis. Our PRM assay meets the requirement of Tier 2 measurement of the Guidelines for Targeted MS Manuscripts of Molecular and Cellular Proteomics journal.

Phosphopeptide Enrichment for PRM Analysis

Phospho-peptide enrichment was performed with Zr-IMAC HP beads (MagReSyn, ReSyn Biosciences). For this, beads were used in 4:1 beads-to-peptide ratio. Zr-IMAC HP beads are magnetic, therefore each supernatant removal step was executed by using a magnetic rack. Beads were equilibrated and washed with loading buffer (80% ACN, 5% TFA, 0.1 M glycolic acid). Dried, tryptic peptides were re-dissolved in a loading buffer (3 min sonication) and added to the Zr-IMAC HP beads. Samples were then incubated at 25 °C for 30 min at 850 rpm. Subsequently, non-phospho-peptides were removed and either discarded or transferred to a fresh Eppendorf tube and dried. Beads were washed in three steps, first adding 500 µl of loading buffer with subsequent incubation of 1 min at 25 °C with 850 rpm, the supernatant was removed and discarded and this step was repeated with wash buffer 1 (80% ACN, 1% TFA) and wash buffer 2 (10% ACN, 0.2% TFA). Phospho-peptides were eluted by adding 150 µl of 1% v/v ammonium hydroxide solution to the beads and 10 min incubation at 25 °C, 850 rpm. Phospho-peptides were then transferred to a fresh Eppendorf tube containing 50 µl 10% v/v TFA. A second elution step was performed in the same manner and the supernatant was added to the Eppendorf tube as well. Phospho-peptides were then dried in the SpeedVac (Thermo Fisher Scientific). For MS/MS analysis, phospho-peptides were re-dissolved in 2% v/v ACN/0.05% v/v TFA. Our assay meets the requirement of Tier 2 measurement of the Guidelines for Targeted MS Manuscripts of Molecular and Cellular Proteomics journal.

Basic Reversed Phase Chromatography

For proteome analysis, TMT6-labeled peptides were separated by basic reversed-phase (bRP) chromatography with an Agilent 1100 series HPLC system (Agilent) equipped with a v C18-X-Bridge column (3.5 µm particles, 1.0 mm inner diameter, 150 mm length; Waters). The HPLC was set to operate at a flow rate of 60 µl/min under basic conditions, with buffer A (10 mM NH_4OH in water, pH ~10) and buffer B (10 mM NH_4OH and 80% (v/v) ACN in water, pH ~10). The column was initially equilibrated with a mixture of 95% buffer A and 5% buffer BA linear gradient ranging from 10% to 36% buffer B was then applied for 34 min, followed by a linear increase to 55% over 8 min and a wash step with 95% buffer B for 5 min. The resulting peptides were collected into 12 final fractions by concatenating one-minute fractions. Finally, the resulting bRP fractions were dried using a SpeedVac.

LC-MS/MS Analysis

Dried TMT-labelled peptides were resuspended in 5% (v/v) ACN, 0.1% (v/v) TFA in water and injected onto a C18 PepMap100-trapping column (0.3 × 5 mm, 5 µM, Thermo Fisher Scientific, Waltham, USA) coupled to a C18 analytical column packed in-house (75 µM × 300 mm, Reprosil-Pur 120C18- AQ, 1.9 µm, Dr Maisch, GmbH, Ammerbuch, Germany). The HPLC system was operated at a flow rate of 0.300 µl/min on an UltiMate-3000 RSLC nanosystem (Thermo Fisher Scientific). Both columns were equilibrated with a mixture of 95% buffer A (0.1% (v/v) FA in water) and 5% buffer B (80% (v/v) ACN, 0.1% (v/v) FA in water). TMT-labelled K-ε-GG peptides were eluted by using a linear gradient ranging from 14% to 38% buffer B for 90 min followed by a linear increase to 48% buffer B for 10 min and a wash step with 90% buffer B for 5 min. The eluted peptides were further injected into a QExactive HF-X (Thermo Fisher Scientific), operated in data-dependent acquisition mode alternating between MS and MS2 acquisitions. TMT-labeled K-ε-GG peptides were analyzed by using the following settings: MS1 scans in the range of 300 to 1400 *m/z* were acquired at a resolution of 120,000 at *m/z* 200, with automatic gain control (AGC) of 10^6 and a maximum injection time of 100 ms. The 20 most abundant precursor ions with a charge state of +2 to +6 were selected using a 0.8 *m/z* isolation window and fragmented with a normalized collision energy (NCE) of 33%. MS2 fragment spectra were acquired with a resolution of 30,000, an AGC target of 10^5, and a maximum injection time of 120 ms. Dynamic exclusion was applied for 20 s and a lock mass ion (*m/z* 445.1200) was used for internal calibration.

For the analysis of peptides not labeled with K-ε-GG TMT, similar settings were used, with the following exceptions: a linear gradient ranging from 10% to 36% buffer B for 62 min followed by a linear increase to 45% buffer B for 8 min was used. The eluted peptides were further injected into an Orbitrap Exploris 480 (Thermo Fisher Scientific), where MS1 scans were acquired in the range of 300 to 1700 *m/z* and with a maximum injection time of 40 ms. The 30 most abundant precursor ions were selected using a 0.7 *m/z* isolation window and fragmented with an NCE of 36%. MS2 fragment spectra were acquired with an AGC target of 5×10^4 and a maximum injection time of 60 ms.

For the PRM analysis of K-ε-GG peptides, similar settings were used, with the following exceptions: a linear gradient ranging from 12% to 36% buffer B for 43 min followed by a linear increase to 45%

buffer B for 3 min was used. The eluted peptides were further injected into an Orbitrap Exploris 480 (Thermo Fisher Scientific), which was operated in targeted mass acquisition mode switching between MS1 and targeted MS2 scans. Within a 3-s cycle time, one MS1 scan in the range of 350 to 1300 *m/z* was acquired with a maximum injection time of 50 ms followed by MS2 spectra derived from the targeted peptides. Specifically, heavy and light peptides matching the *m/z* values defined in the precursor isolation list were isolated with a 1 *m/z* isolation window and fragmented with a normalized collision energy (NCE) of 28%. MS2 fragment spectra were acquired with a resolution of 60,000, an AGC target of 5×10^5, and a maximum injection time of 120 ms.

Peptide Identification and Data Analysis

Raw files were analyzed by using the MaxQuant (MQ) software (version 2.0.3.0) (43, 44). Precursor ions and MS2 spectra were searched against the proteome of *R. norvegicus* containing canonical protein sequences (Uniprot (45), March 2021, 29,942 entries). Most of the MQ search settings were kept at default, with the following exceptions; apart from the default variable and fixed modifications (methionine oxidation, acetylation of protein N-termini, and cysteine carbamidomethylation) K-ε-GG of lysine and TMT-6plex of lysine were set as variable modifications (only for the K-ε-GG peptides). Specific digestion with trypsin was selected allowing up to three missed cleavage sites per peptide. The maximum peptide mass was set to 5000. Precursor and fragment ion mass tolerances were kept at 4.5 ppm and 20 ppm, respectively. For K-ε-GG peptide quantification, reporter ions in MS2 level were selected with TMT6plex of the peptide N-termini as isobaric labels, whereas for non-K-ε-GG peptide quantification, TMT6plex values of the peptide N-termini and internal lysines were determined as isobaric labels. FDR at the PSM and protein levels were kept at the default setting of 1%.

All the downstream data analysis was performed in R statistical programming language using customized scripts. Impurity-corrected reporter ion intensities for each ubiquitination site were retrieved from the MaxQuant K-ε-GG site table. Ubiquitination sites assigned to potential contaminants, reversed sequences, or with a localization probability lower than 0.75 as estimated by MQ were not considered in the downstream analysis. Ubiquitination sites with more than three zero values per TMT-6plex experiment were excluded from the quantification analysis. The remaining zero values (if any) were imputed using the minimal reporter ion intensity per channel. Corrected reporter ions were $\log_2$-transformed and normalized by using the Tukey median polishing procedure with a maximum iteration number of three. Finally, statistical testing was conducted using the limma package (46).

Gene enrichment analysis was performed using the synapse-specific database, SynGO (SynGO release 20210225) (47) and ShinyGO (release version 0.77). Gene names of proteins associated with ubiquitination sites were used as the foreground against a custom "synaptic proteome" background to extract significantly enriched (FDR corrected p value < 0.001) GO-biological process terms. An experimentally validated ubiquitination site data set downloaded from PhosphoSitePlus (48) (February 2023) containing 105,710 unique ubiquitination sites was used as a literature reference and compared with our data set. Sequence windows of the ubiquitination sites in our data set were aligned against sequence windows in the PhosphoSitePlus data set with Blast software (49) (version 2.13.0+), to account for possible sequence differences across different species.

PRM Data Analysis

PRM raw data files were imported into Skyline (50) (version 21.2.0.369) for manual inspection and refinement of integrated peak areas. Only peptides with at least 7 transitions were further considered for the quantification analysis. For quantification, low-intensity transitions were not considered, and the peak areas of selected transitions were summed, as determined by Skyline (50). Summed peak areas of endogenous peptides were normalized to summed peak areas of heavy peptides, as determined by Skyline (50). Normalized peak area ratios were exported from Skyline and further subjected to statistical analysis in R using the limma package.

Cell Culture and Generation of CaMKIIα WT and CaMKIIα K291R HeLa Kyoto Cell Lines

HeLa Kyoto cells were cultured in high glucose Dulbecco's modified Eagle's medium (DMEM, Gibco, Thermo Fisher Scientific) supplemented with 10% fetal bovine serum (FBS), 2 mM glutamine, 1 mM sodium pyruvate, and 100 units/ml penicillin, 0.1 mg/ml streptomycin at 37 °C and 5% CO_2. Two different cell lines were generated: 1 cell line expressing wild-type CaMKIIα and another expressing the mutant variant CaMKIIα K291R. For this purpose, HeLa Kyoto cell lines were transfected with the Lipofectamine 3000 kit (Invitrogen, Thermo Fisher Scientific) and cells stably expressing the constructs 2 days after transfection were selected with 500 μg/ml geneticin (Gibco, Thermo Fisher Scientific).

Experimental Design and Statistical Rationale

In a discovery approach, two TMT6 labeling experiments were performed to quantify changes in ubiquitination site and protein intensities in synaptosomes stimulated under different conditions (Ca^{2+} *versus* EGTA). Each set of TMT6-labelled samples included three independent replicates for each of the two treatment conditions, yielding a total of six independent replicates. For the proteome analysis, 24 raw files were obtained from two independent TMT6 labeling experiments, corresponding to 12 concatenated bRP-fractions for each TMT6 labeling experiment. For the quantification of ubiquitination site intensities, 4 raw files were obtained from two independent TMT6 labeling experiments and 2 injection replicates per TMT6 labeled samples. The corrected reporter ion intensities obtained from the two injection replicates were summed and a single value was determined using MaxQuant (44). All downstream statistical tests were performed in R using the limma (46) and q-value packages as previously described (13) with some modifications. Briefly, the reporter ion intensities for each TMT6 labeling experiment were independently $\log_2$ transformed and normalized. For each TMT6 labeling experiment, the resulting normalized values were used to test the significance of changes using the limma package. Linear models were fitted to account for the different treatment conditions. The resulting empirical Bayes moderated p-values (46) were corrected for multiple testing using the q-value approach (51). Finally, the normalized values from both experiments were considered together and tested for significant changes using the method described above. Ubiquitination site intensities showing at least 1.15-fold change and a q-value <0.05 were considered significantly changed.

PRM-MS analysis was used to validate the changes in ubiquitination site intensities in depolarized synaptosomes under different stimuli. A total of 46 raw files were obtained from 2 independent experiments and three injection replicates per experiment. Each experiment included three independent replicates for each treatment condition, resulting in a total of six replicates per experiment. Light-to-heavy peptide intensity ratios as determined by Skyline (50) were used to assess significant changes. Specifically, the mean of light-to-heavy peptide intensity ratios resulting from three injection replicates was determined and a single value was used for the limma (46) statistical test as described above. Linear models were fitted to account for treatment conditions and batch effects between different experiments. Ubiquitination site intensities showing at least a 1.23-fold change and a q-value <0.05 were considered significantly changed.

Finally, to quantify changes in ubiquitination at K291 and phosphorylation at T286 of CaMKIIα in stimulated synaptosomes and HeLa cells under different conditions 92 raw files were obtained in a targeted acquisition mode. In synaptosomes, 46 raw files were obtained from two independent experiments and two injection replicates per experiment. Each experiment contained three and four independent replicates for the Ca^{2+} and EGTA treatment, respectively. Each of these samples was split in half, with one half treated with the QuickCIP phosphatase and the other half untreated, resulting in 14 samples per experiment. Light-to-heavy peptide intensity ratios were reported by Skyline (50) and the statistical tests were performed as described above. The remaining 36 raw files were obtained from two independent experiments in stimulated HeLa cells and two injection replicates per experiment. One experiment was performed to quantify the changes in CaMKIIα T286 autophosphorylation in two different cell lines (WT *versus* CaMKIIα K291R mutant) in the presence of ionomycin or DMSO. Three independent replicates for each treatment condition were used for each cell line. The other experiment was performed to quantify changes in CaMKIIα K291 ubiquitination in HeLa cells under different conditions (ionomycin vs. DMSO). Three independent replicates were used for each treatment condition. Light-to-heavy peptide intensity ratios were reported by Skyline (50) and a two-sample *t* test was performed to determine significant differences.

HeLa Cell Processing Prior to PRM-MS Analysis

HeLa cells stably expressing CaMKIIα were stimulated with 2.5 μM of the calcium ionophore, ionomycin (Sigma Aldrich) in the presence of 1.8 mM $CaCl_2$ in a cell incubator at 37 °C, and 5% CO_2 for 7 min. Then, the medium was discarded, and the cells were washed one time with PBS (Company, Cat#), followed by the addition of lysis buffer (0.5% v/v NP40, 50 mM HEPES, pH 7.5, 100 mM NaCl, 1 mM EDTA; 50 μM PR-619, 40 mM CAA, 1× Halt protease and phosphatase inhibitor cocktail). Cells were scraped off and the cell lysates were transferred to tubes. Nuclei were pelleted by centrifuging at 10,000*g* for 30 s at 4 °C in a bench-top centrifuge. The supernatants were transferred to new tubes and any remaining DNA was further digested by the Pierce universal nuclease (250 U) (Thermo Fisher Scientific) in the presence of 4 mM $MgCl_2$ for 30 min at 37 °C. Subsequently, 20 mM TCEP/40 mM CAA were added to the solutions followed by incubation for 30 min at 37 °C to reduce disulfide bonds and carbamidomethylate cysteine residues. Afterward, equal amounts of proteins as determined by the BCA assay were cleaned up by the single-pot, solid-phase-enhanced sample-preparation (SP3) method as previously described (52) with a few modifications. Specifically, 10 mg of the bead stock (Sera-Mag Speedbeads, Cytiva) per 1 mg of protein solution. To induce binding of the proteins to the beads 100% ACN was added to the solution to achieve a final ACN concentration of 50% v/v. The binding mixture was incubated at 24 °C for 5 min at 1000 rpm. Afterwards, the tubes were placed in a magnetic rack and the unbound fraction was discarded. Afterward, beads were washed three times with 80% v/v ethanol. A final washing step was performed with 100% v/v ACN. Beads were resuspended in a digestion buffer (100 mM TEAB) and sonicated for 2 min in a water bath. Finally, proteins were digested for 16 h at 25 °C with trypsin at a trypsin-to-protein ratio of 1:30 (w/w). The next day, the tubes were placed in the magnetic rack and peptide solutions were collected into fresh tubes. 700 fmol of standard synthetic AQUA peptides per mg of protein amount (Technologies, Thermo Fisher Scientific) were added to the endogenous peptide mixture and peptides were dried in a centrifugal Savant SpeedVac (Thermo Fisher Scientific). Dried peptides were used either for K-GG peptide enrichment or phosphopeptide enrichment as previously described before, respectively, prior to PRM-MS analysis.

Preparation of Rat Dissociated Hippocampal Cultures

Newborn rats were used for the preparation of dissociated primary hippocampal cultures, as previously described (53). In brief, hippocampi of newborn rat pups (wild-type, Wistar) were dissected in Hank's Buffered Salt Solution (HBSS, 5 mM KCl, 140 mM NaCl, 4 mM NaHCO3, 0.3 mM Na2HPO4, 6 mM glucose and 0.4 mM KH2PO4). Subsequently, the tissues were incubated for 1 h in an enzyme solution (Dulbecco's Modified Eagle Medium, DMEM, #D5671, Sigma-Aldrich), containing 0.5 mg/ml cysteine, 50 mM EDTA, 100 mM CaCl2, and 2.5 U/ml papain, saturated with carbogen for 10 min). The dissected hippocampi were then incubated for 15 min in a deactivating solution (DMEM with 0.2 mg/ml bovine serum albumin, BSA, 5% fetal calf serum, and 0.2 mg/ml trypsin inhibitor). Then the cells were triturated and seeded at a density of about 80,000 cells per 18 mm round coverslip. Before seeding, the coverslips underwent a treatment with nitric acid, then they were sterilized and coated overnight with 1 mg/ml poly-L-lysine. The cells were allowed to attach to the coverslips for a period between one to 4 h at 37 °C in a plating medium (DMEM with 10% horse serum, 2 mM glutamine, and 3.3 mM glucose). The plating medium was then replaced with a Neurobasal-A medium (Life Technologies, Carlsbad) containing 1% GlutaMax (Gibco, Thermo Fisher Scientific), 2% B27 (Gibco, Thermo Fisher Scientific) supplement, and 0.2% penicillin/streptomycin mixture (Biozym Scientific). Before use, the cultures were maintained in a cell incubator at 37 °C, and 5% CO2 for 9 to 11 days. Percentages represent volume/volume.

Transfection of Hippocampal Neurons

Transfections were performed with a standard Lipofectamine 2000 kit (#11668019, ThermoFisher Scientific). In brief, neurons were pre-incubated for 25 min in 400 μl per well, pre-heated DMEM (#D5671, Sigma-Aldrich) complemented with 10 mM MgCl2 at pH 7.5 (fresh-DMEM). Per 18 mm coverslip, one 1 μg of DNA, prepared in a total volume of 25 μl Opti-MEM (#11058-021, Life Technologies Limited) was used. The DNA-Opti-MEM solution was incubated for 5 min and added to 25 μl Opti-MEM with 1 μl lipofectamine solution. Then the solution was incubated for 15 min and subsequently added to the neurons. After incubating the neurons at 37 °C and 5% CO2 for 20 min, they were washed 2 times with fresh-DMEM, returned to their original culture medium, and incubated at 37 °C and 5% CO2 until the conduction of the respective experiments.

Live Labelling and Fixation

Cells were incubated live with 1:200 monoclonal mouse anti-Synaptotagmin1 antibody, conjugated to ATTO647N (#105 311AT1, Synaptic Systems) for 60 min at 37 °C and 5% CO2. After three washes with Tyrode's solution (124 mM NaCl, 30 mM glucose, 25 mM HEPES, 5 mM KCl, 1 mM MgCl2, 2 mM CaCl2, pH 7.4), the cells were fixed in 4% PFA in PBS (10 mM Na2HPO4, 137 mM NaCl, 2.7 mM KCl, 2 mM KH2PO4, pH 7.4) for 20 min at room temperature. The fixation reaction was quenched with 100 mM NH4Cl in PBS for 20 min. For subsequent immunostainings, neurons were permeabilized and blocked with PBS containing 0.1% Triton X (#9005-64-5, Merck), 5%, bovine serum albumin (BSA) (#A1391-0250; Applichem) for 30 min.

Imaging and Image Analysis

The neurons were imaged with an inverted Nikon Ti microscope (Nikon Corporation) with a Plan Apochromat 60× objective (1.4 NA, immersion oil). For the image analysis, a custom-made Matlab (Matlab version 2022b, the Mathworks Inc) macro was used. Briefly, synapses were identified based on the Syt1 signal. The fluorescence signal of

Syt1 in the synaptic boutons was correlated with the CaMKIIα expression signal within the area of each synapse, using Pearson correlation. Subsequently, the fluorescence intensity of Syt1 was quantified in the boutons in which the Syt1 and the CaMKIIα signals correlated well. A paired *t* test between the wild type and the mutant was performed to determine significant differences ($p = 0.03$).

RESULTS

Description of the Workflow and Overview of Results

In a first discovery approach, we performed a quantitative analysis of ubiquitinated proteins in chemically stimulated synaptosomes under Ca^{2+}-restricted and Ca^{2+}-rich conditions (Fig. 1). Membrane depolarization of synaptosomes was chemically induced by increasing the external concentration of KCl in the medium. To assess whether synaptosomes were responsive to chemical depolarization the release of glutamate was monitored upon stimulation as previously described (37) (supplemental Fig. S1*A*). Chemical depolarization was applied for 2 min in a buffer containing either the Ca^{2+} chelator EGTA or Ca^{2+} (Fig. 1). Subsequently, equal amounts of protein from differentially treated synaptosomes were precipitated and sequentially digested with LysC and trypsin. Tryptic digestion of ubiquitinated proteins leaves a ubiquitin-remnant di-glycine dipeptide on the lysine residue of the substrates (K-ε-GG) with a monoisotopic mass of 114.04 Da. We used commercially available antibodies that specifically recognize the ubiquitin remnant to enrich for K-ε-GG peptides. Following enrichment, the proportion of peptides bearing ubiquitination remnants reached 85% and 98% in two independent experiments, respectively, demonstrating the high specificity of the immunoaffinity enrichment approach (supplemental Fig. S2*C*). Subsequently, the K-ε-GG peptides were chemically labeled with TMT6 reagents, combined, and analyzed by LC-MS/MS (Fig. 1). In parallel, we compared the proteome of depolarized synaptosomes under Ca^{2+}-restricted and Ca^{2+}-rich conditions using TMT-based quantification approach, followed by off-line basic reversed phase (bRP) peptide fractionation and LC-MS/MS analysis.

Our analyses led to the identification and quantification of 5258 confidently localized ubiquitination sites in more than 2000 proteins, demonstrating that ubiquitination is a widespread post-translational modification of synaptic proteins covering a wide range of protein abundances in our samples, which include both Ca^{2+}-treated and EGTA-treated synaptosomes (Fig. 2*A*). Our data represent a unique data set of ubiquitination sites in the synapse. Many synaptic proteins were found highly ubiquitinated at more than 20 sites, such as synaptotagmin-1 (*Syt1*), Munc-18 (also known as *Stxbp1*) and CaMKIIα (Fig. 2*A*). Comparison of our ubiquitination data set with a previous data set derived from whole mouse brain revealed more than 2000 shared ubiquitination sites (35) (Fig. 2*D*). A similar comparative analysis of our data set with the PhosphositePlus ubiquitination data set (48) showed that 65% of the ubiquitination sites identified by us have been previously reported in other studies. Our data set thus encompasses hitherto non-identified ubiquitination sites, such as four distinct sites in the C-terminal region of the AZ protein, RIM, a well-established substrate of ubiquitination (22) (supplemental Fig. S3*A*), 12 novel sites mapped to the AZ protein piccolo (*Pclo*), four novel sites in complexin, and five novel sites mapped to the SNARE protein syntaxin-1 (*Stx1*) (supplemental Data S1). Finally, the proteomic analysis resulted in the identification and quantification of approximately 5800 unique proteins, hereafter referred to as the "synaptic proteome" of our sample, which was used as a true positive background in the pathway enrichment analysis (see below).

To obtain an overview of the functional properties of the identified ubiquitinated proteins we performed pathway enrichment analysis using SynGO, a synapse-specific database containing high-quality annotations (47). Among the identified ubiquitinated proteins, 558 were mapped to unique annotated genes in the SynGO database (47). Subsequent enrichment analysis of these ubiquitinated proteins using our "synaptic proteome" as a custom background proteome revealed significantly enriched terms primarily associated with presynaptic functions such as the SV cycle, SV exo- and endocytosis (Fig. 2, *A* and *B*). Even though SynGO is a synapse-specific database with high-quality annotations, it contains annotation exclusively for synaptic proteins. To obtain a more comprehensive view of the functional properties of ubiquitinated proteins, we performed a pathway enrichment analysis using ShinyGO, which uses annotations from the Ensembl database (54) (Fig. 2*C*). Consistent with SynGO, enrichment analysis using ShinyGO revealed significantly enriched terms associated with synaptic functions including SV cycle, vesicle-mediated transport in the synapse, regulated exocytosis etc (Fig. 2*C*). In addition to synaptic functions, ShinyGO enrichment analysis also revealed significantly enriched terms associated with the enzymatic machinery necessary for ubiquitination (Fig. 2*C*). In particular, the term "regulation of proteasomal protein catabolic process" includes ubiquitin ligases as well as DUBs, which are of interest, as they may contribute to synapse-specific ubiquitination patterns (supplemental Tables S7 and S8). For a detailed list of enriched GO terms, see supplemental Tables S2 and S3.

Changes in Protein Ubiquitination in Depolarized Synaptosomes

A quantitative comparison of the ubiquitination sites of chemically depolarized synaptosomes under Ca^{2+}-deprived and Ca^{2+}-rich conditions demonstrated that only a small fraction of ubiquitination sites changed significantly in response to Ca^{2+} influx. Specifically, our quantitative analysis revealed 43 ubiquitination sites associated with 41 proteins that showed at least a 1.15-fold change at a false discovery rate (FDR) of 5% (Fig. 3*A*). Both ubiquitination and deubiquitination events were observed, with deubiquitination events

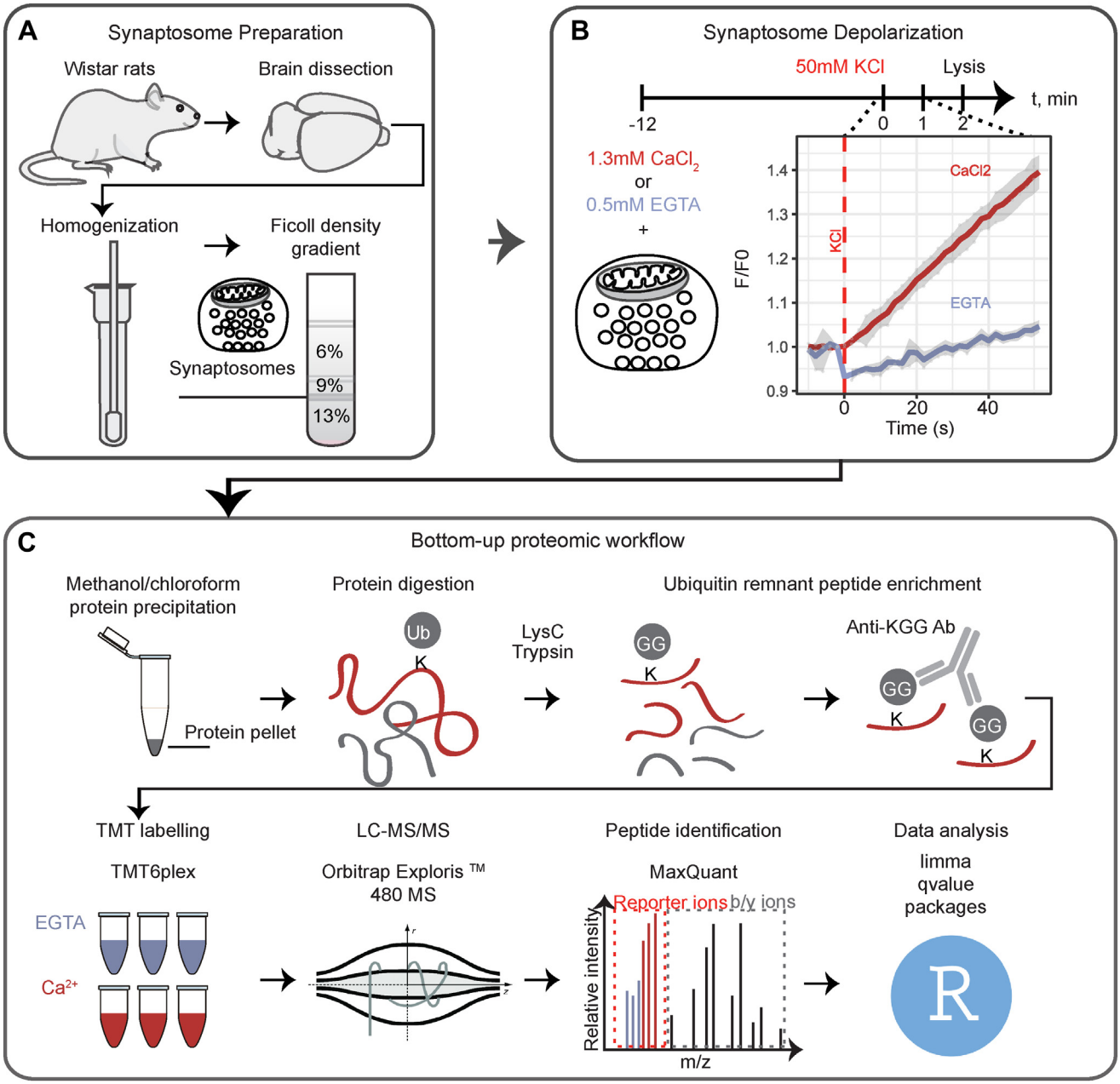

Fig. 1. **Workflow for the quantitative analysis of ubiquitinated proteins in depolarized synaptosomes under different conditions**. *A*, synaptosomes were isolated from the brains of 5–6-week-old Wistar rats by homogenization of brain tissue followed by differential centrifugation and discontinuous Ficoll gradient centrifugation. *B*, synaptosome depolarization was induced by KCl in the presence of Ca^{2+} or the Ca^{2+}-chelator EGTA and was quenched after 2 min by the addition of lysis buffer. Three independent stimulations were performed for each condition (EGTA *versus* Ca^{2+}). *C*, equal amounts of proteins were subsequently precipitated by methanol/chloroform protein precipitation and sequentially digested with LysC and trypsin, followed by ubiquitin remnant-containing (K-ε-GG) peptide enrichment and chemical labeling with isobaric TMT6 reagents. Differently labeled peptides were combined and analyzed by LC-MS/MS. Two independent TMT6 experiments were performed. Peptide identification and quantification was performed in MaxQuant and the extracted reporter ion intensities were further processed in R.

being slightly more pronounced. This is consistent with the results of a previous study demonstrating a decrease in total ubiquitination levels in response to chemical depolarization (26). We note that we do not observe a change in the abundance of the ubiquitin chains of different linkage types upon stimulation, as reflected by the corresponding di-glycine-modified remnants on ubiquitin itself.

To obtain an overview of the functional characteristics of proteins with regulated ubiquitination sites, we performed a pathway enrichment analysis using the SynGO database (47).

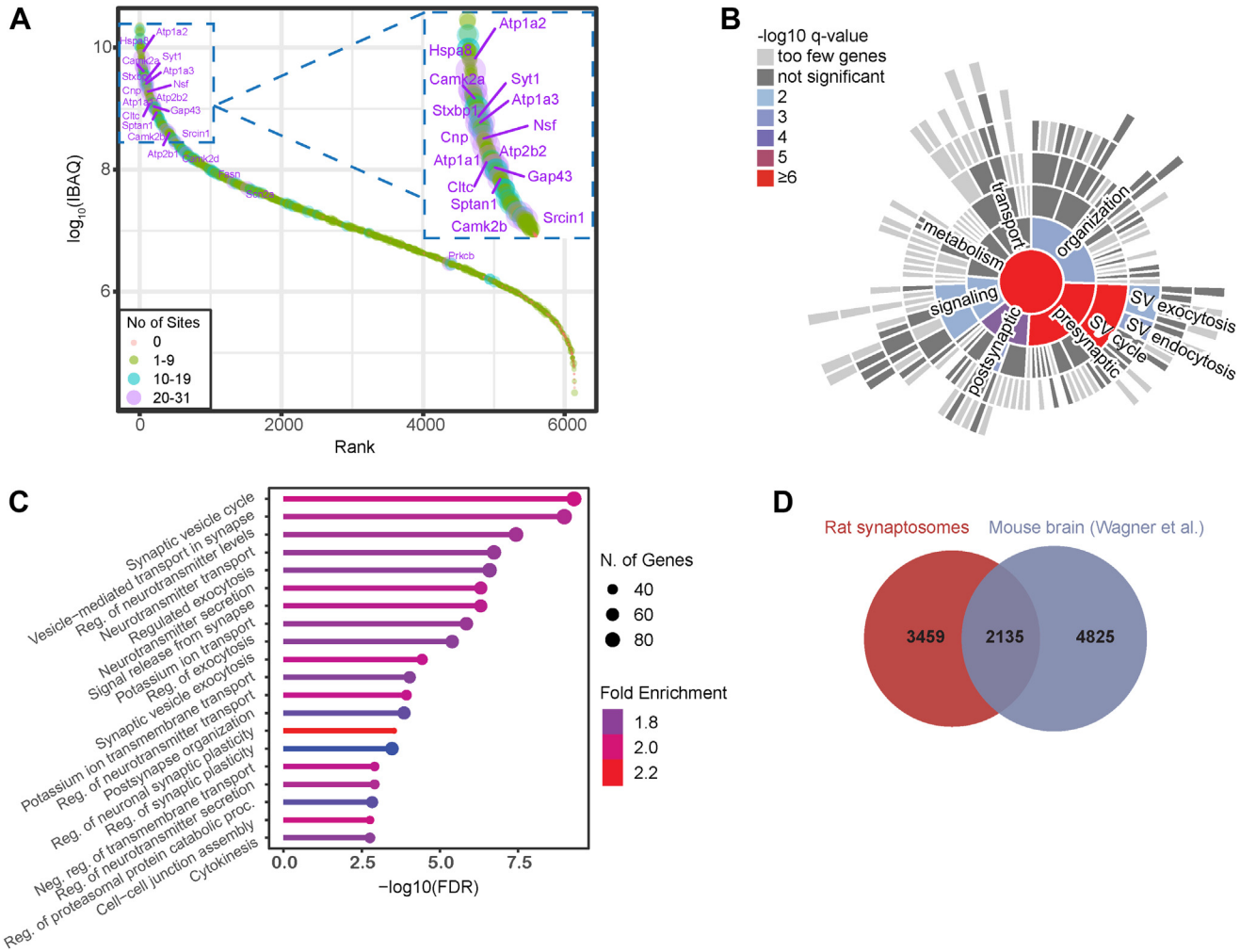

FIG. 2. **Pathway enrichment analysis of ubiquitinated proteins identified in synaptosomes and comparison of our data set with the literature**. *A*, rank order of protein signals depicting the number of identified ubiquitination sites per protein in our samples, which include both Ca^{2+}- and EGTA-treated syntaptosomes. *B*, sunburst diagram depicting significantly enriched biological process terms based on the SynGo database (47). *C*, detailed list of enriched biological processes based on the ShinyGO (54). *D*, comparison of our ubiquitination data set derived from rat synaptosomes with a previous ubiquitination data set derived from mouse brain (35) based on sequence similarity of the six amino acids flanking N- and C-terminal the modified lysine residue.

Of the 41 proteins with regulated ubiquitination sites, only 18 were mapped to the SynGO database. Enrichment analysis with our "synaptic proteome" as a background revealed enriched terms associated primarily with presynaptic functions, namely, SV exo- and endocytosis as well as dense core vesicle exocytosis (Fig. 3*B*). Specifically, proteins involved in SV endocytosis, such as AP180, EPS15L and Pip5k1c, were found to undergo deubiquitination in response to Ca^{2+} influx, with the clathrin adaptor protein AP180 showing the most prominent change (Fig. 3*A*). Interestingly, the downregulated ubiquitination site of AP180 was mapped to K28, within the AP180 N-terminal homology (ANTH) domain (55, 56) (supplemental Fig. S3*B*). Like AP180, Ca^{2+}/calmodulin-dependent kinase 2α (CaMKIIα) underwent a drastic decrease in its ubiquitination state in response to depolarization (Fig. 3*A*). The downregulated ubiquitination site of CaMKIIα was mapped to K291 within the regulatory domain (*i.e.*, the autoinhibitory domain) of CaMKIIα (supplemental Fig. S3*C*). Conversely to endocytic proteins, active zone (AZ) proteins—such as Cadps1, Munc-18 (also known as *Stxbp1*), and synaptotagmin-7 (*Syt7*)—show enhanced ubiquitination upon stimulation (Fig. 3, *A* and *B*).

To validate differentially regulated ubiquitination sites, instead of "classical" orthogonal approaches (*e.g.* Western blot analysis) we adopted a targeted MS approach, *i.e.* parallel reaction monitoring (PRM) (57) (Fig. 3C). PRM relies on synthetic isotope-labeled standard peptides that are added to the mixture of endogenous peptides in known amounts, thus allowing the (modified) endogenous peptide to be monitored quantitatively. Using synthetic isotope-labeled and modified

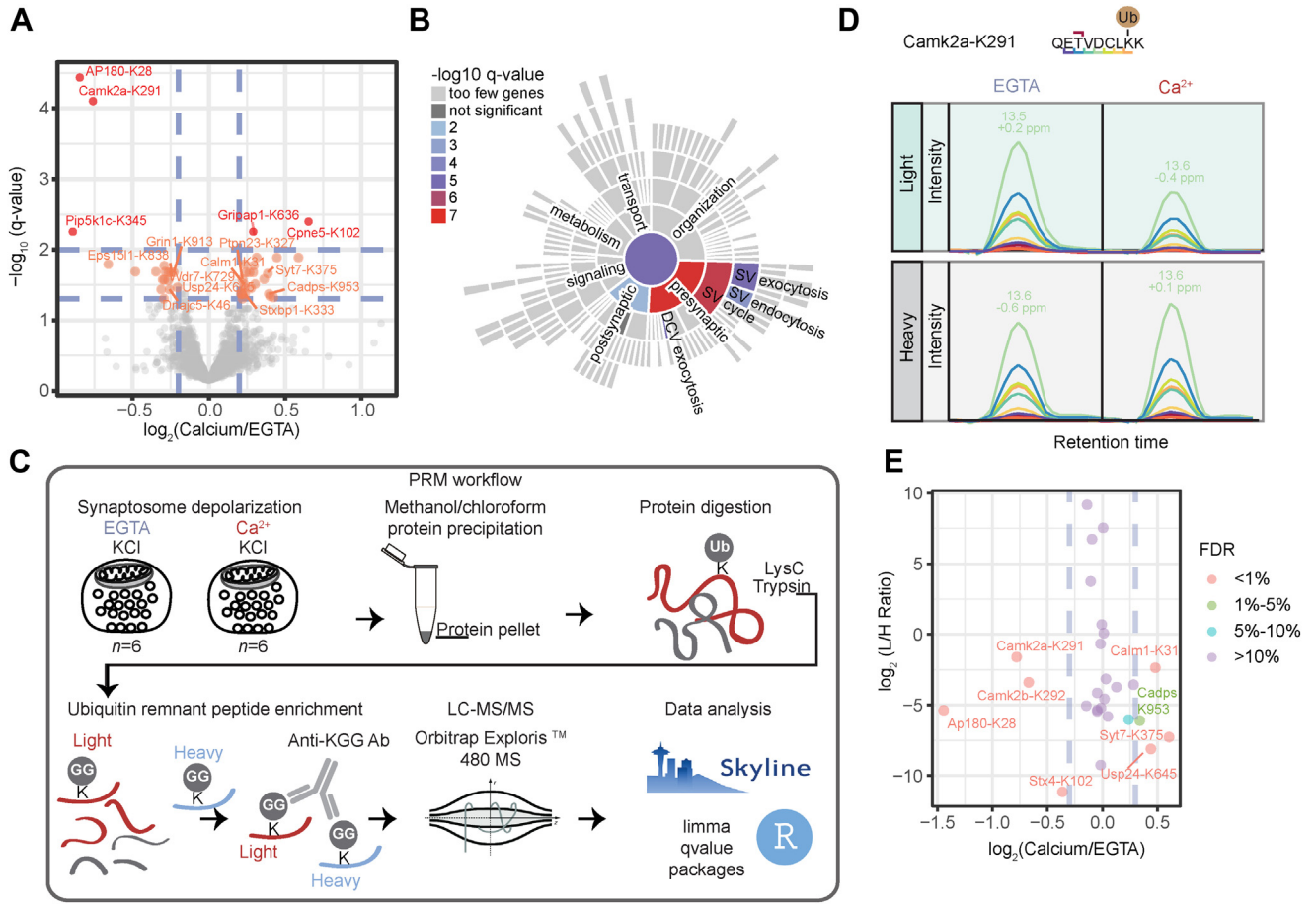

FIG. 3. **Ubiquitination changes in depolarized synaptosomes under different stimuli**. *A*, volcano plot showing $\log_2$(intensity fold change) of ubiquitination sites quantified under Ca^{2+} vs. EGTA conditions against $-\log_{10}$(q-value). The color encodes the significance of changes, highlighting with red and orange the ubiquitination sites that change significantly at FDRs of 1% and 5%, respectively. *B*, sunburst diagram depicting enriched biological process terms of proteins possessing regulated ubiquitination sites based on the SynGO database (47). *C*, synaptosome depolarization was induced by KCl in the presence of Ca^{2+} or the Ca^{2+}-chelator EGTA and was quenched after 2 min by the addition of lysis buffer. Six independent stimulations were performed for each condition (EGTA *versus* Ca^{2+}). Equal amounts of proteins were subsequently precipitated by methanol/chloroform protein precipitation and sequentially digested with LysC and trypsin. Standard/heavy peptides were spiked in the mixture of endogenous/light peptides prior to ubiquitin-remnant (K-ε-GG) peptide enrichment. Eluted (K-ε-GG) peptides were analyzed by LC-MS/MS. Peptide identification and quantification were performed in Skyline and the extracted peak areas were further processed in R. *D*, representative extracted fragment ion chromatograms for endogenous/"light" and standard/"heavy" CaMKIIα peptide (QETVDCLKK) ubiquitinated at K291, under calcium-deprived (EGTA) and calcium-free conditions. The different colors represent distinct fragments b and y ions of the indicated peptide. *E*, Log_2(light-to-heavy peptide intensity fold change) of ubiquitination sites quantified under Ca^{2+} vs. EGTA conditions against the average $\log_2$ (light-to-heavy peptide intensity ratio) for the Ca^{2+} and EGTA conditions. The color shows the statistical significance (FDR) of $\log_2$(light-to-heavy peptide intensity fold change).

peptides with the ubiquitin remnant at the lysine position, we targeted in total nine regulated and 17 non-regulated ubiquitination sites according to the TMT experiment (supplemental Tables S4, supplemental Datas 3.1, and 3.2), including K-ε-GG peptides derived from ubiquitin itself (Fig. 3*C*). Our analysis validates six out of nine selected regulated sites, and 14 out of the 17 non-regulated ubiquitination sites, demonstrating the capacity of PRM as an additional validation strategy to reveal false positive and false negative hits (Fig. 3*E* and supplemental Data S4). We consider the $\log_2$ fold change values (log2FC) determined by the PRM approach to represent the "true" values, as PRM is more accurate and does not suffer from ratio compression inherent to the TMT-labelling method (58). Indeed, by comparing the log2FC obtained using PRM with those from the TMT-labeling method, we observed a general trend of ratio compression in the TMT data (supplemental Fig. S4). Specifically, the TMT method tends to underestimate the log2FC values by a factor of 1.43 (as indicated by the slope of the regression line in supplemental Fig. S4).

Importantly, we confirmed the stark deubiquitination events on K28 of AP180 and K291 of CaMKIIα upon stimulation.

Specifically, the ubiquitination of AP180 showed a decrease by a factor of 2.8, whereas the ubiquitination of CaMKIIα showed a decrease by a factor of 1.7. We do not attribute these fast and drastic changes in the ubiquitination pattern that we (and others (26)) observe to protein degradation for several reasons: first, we (and others) observe a rapid (within seconds to 2 min) deubiquitination upon depolarization of synapses; second, we do not observe a change in the abundance of the corresponding proteins, AP180 and CaMKIIα (supplemental Fig. S1*B*); and third, AP180 and CaMKIIα are unusually long-lived, with average respective lifetimes of 52 and 16 days in cortex synaptosomes (59).

The Regulatory Region of CaMKIIα is a Hotspot of PTMs

Our quantitative analysis revealed that CaMKIIα undergoes marked deubiquitination at K291 in response to stimulation, an observation that was further validated by our PRM analysis. This finding is interesting for several reasons: First, the ubiquitination site (K291) resides in the autoinhibitory domain of CaMKIIα, which is critical for regulating the enzyme's activity (60, 61) (Fig. 4*A*). Second, K291 is located close to a regulatory autophosphorylation site of CaMKIIα, T286, which when phosphorylated confers Ca^{2+}-independent activity to the enzyme (62, 63). Third, sequence comparison reveals that K291 is highly conserved among metazoan from cnidarians to humans, as well as conserved within the CaMKIIα paralogue genes α, β, and δ, suggesting its functional importance (supplemental Fig. S5*A*). Lastly, the deubiquitination of CaMKIIα at K291 is reversible upon Ca^{2+}-chelation, indicating a potential modulatory role of ubiquitin (supplemental Fig. S5*C*).

It is well established that CaMKIIα undergoes activation upon Ca^{2+}-influx, exposing T286 for trans autophosphorylation by neighboring CaMKIIα subunits of the multimeric structure (64) (Fig. 4*B*). Accordingly, CaMKIIα was reported to undergo phosphorylation at T286 in depolarized synaptosomes upon Ca^{2+} influx (13). Importantly, the regulatory autophosphorylation (T286) and ubiquitination (K291) sites are located within the same tryptic peptide, which was analyzed by MS. As CaMKIIα phosphorylation increases with stimulation, the singly ubiquitinated form can be converted into the doubly modified ubiquitinated-phosphorylated form, resulting in a measurable decrease in the levels of the singly ubiquitinated peptide (Fig. 4*C*). In an extreme theoretical example, illustrated by Figure 4*C*, if all ubiquitinated molecules of CaMKIIα are phosphorylated at T286 during stimulation, then we should detect a 100% decrease in the levels of the ubiquitinated peptide, although its ubiquitination status remained unchanged.

Indeed, when we considered both ubiquitin remnant (K-ε-GG) on lysine residues and phosphorylation on threonine residues as variable modifications we observed this reciprocal relationship: decreased levels of the singly ubiquitinated peptide (QETVDCLKggK) and increased levels of the doubly modified form (QETpVDCLKggK) upon stimulation (supplemental Fig. S5*D*). This suggests that the apparent decrease in CaMKIIα ubiquitination at K291 observed during stimulation may be caused (at least in part) by the Ca^{2+}-induced autophosphorylation at T286, which effectively converts QETVDCLKggK into QETpVDCLKggK. This phenomenon exemplifies how co-occurring post-translational modifications within a given peptide can influence quantitative MS analyses, and it should also be considered in other cases (*i.e.*, when comparing synaptic proteins in resting and depolarised synapses; see Discussion).

To determine whether the observed decrease in the ubiquitinated peptide is directly linked to stimulation-induced phosphorylation, we performed an absolute quantification of the relevant peptides in depolarized synaptosomes, using PRM analysis with stable isotope-labeled peptide standards. Specifically, we quantified the absolute amounts of singly ubiquitinated (QETVDCLKggK) and the doubly modified ubiquitinated-phosphorylated (QETpVDCLKggK) peptides of CaMKIIα (supplemental Table S5, supplemental Datas 3.3, and 3.4), following K-ε-GG peptide enrichment. The analysis showed that upon stimulation the absolute levels of the doubly modified peptide (QETpVDCLKggK) increased from a light-to-heavy ratio of 0.034 to 0.1 (Fig. 4, *D* and *E*, supplemental Fig. S5*E*, and supplemental Data S5), while the levels of the singly ubiquitinated peptide (QETVDCLKggK) decreased from a light-to-heavy ratio of 0.27 to 0.14 (Fig. 4, *D* and *E*, supplemental Fig. S5*E*, and supplemental Data S5). These PRM data demonstrate that deubiquitination of the singly ubiquitinated peptide is stronger than the increase in the doubly modified peptide. We thus conclude that the apparent decrease in CaMKIIα ubiquitination is, indeed, due to active deubiquitination at K291 during stimulation.

To further confirm this, we treated the peptide mixture (containing both QETVDCLKggK and QETpVDCLKggK) with phosphatase (PPtase). This treatment selectively removes phosphorylation from QETpVDCLKggK, converting it back into the singly ubiquitinated peptide QETVDCLKggK. By eliminating the confounding factor of phosphorylation, this approach allowed us to quantify the singly ubiquitinated peptide independently of its phosphorylation state (Fig. 4*D*). After phosphatase treatment, the levels of the singly ubiquitinated peptide increased compared to untreated samples in the Ca^{2+} condition (Fig. 4, *D* and *E*). However, these levels still showed a 1.28-fold decrease compared to the EGTA condition (Fig. 4, *D* and *E*, supplemental Fig. S3*E*, and supplemental Data S5). This supports the conclusion that CaMKIIα undergoes deubiquitination at K291 during stimulation.

A ubiquitination-deficient form of CaMKIIα at K291 enhances CaMKIIα T286 autophosphorylation and synaptic function

Our quantitative MS analysis demonstrates that the regulatory domain of CaMKIIα is a target for ubiquitination upon

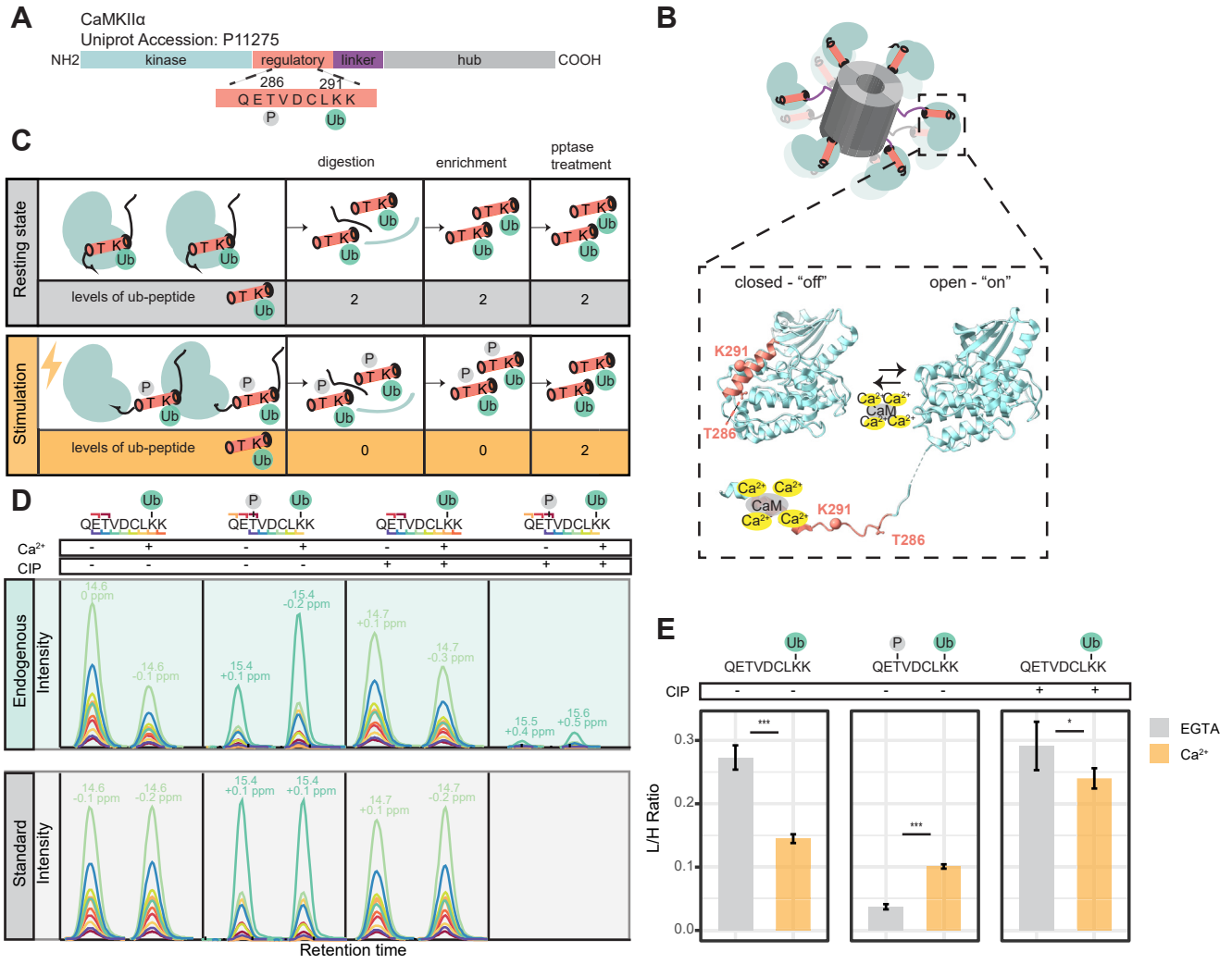

FIG. 4. **PTMs on the regulatory domain of Ca2+/calmodulin dependent kinase II α (CaMKIIα) and their quantification in depolarized synaptosomes under different conditions**. *A*, a horizontal bar represents the CaMKIIα sequence, with colored regions showing the domains annotated according to Chao *et al.*, 2011 (76). The regulatory ubiquitination site (K291) resides in the regulatory domain of CaMKIIα very close to the autophosphorylation site (T286). *B*, dodecameric structure of CaMKIIα and the conformational states of a CaMKIIα subunit; in the closed conformation (PDB code 2VN9 (78)) the regulatory domain folds back to the kinase domain, blocking access to the active site of the enzyme. The binding of Ca2+/calmodulin to the regulatory segment releases the active site of the enzyme, rendering the enzyme catalytically active and T286 accessible for phosphorylation (PDB code 2WEL (78)). Part of the K291 structure represented by a sphere is missing in the PDB codes. The PDB codes correspond to the human CaMKIIδ subunit 0 to 310 aa, which shares 92.58% sequence identity with human CaMKIIα and therefore we can safely assume that these domains have the same structure. *C*, theoretical example where all ubiquitinated molecules of CaMKIIα are phosphorylated at T286 during stimulation, leading to a 100% decrease in the levels of the ubiquitinated peptide. Phosphatase (pptase) treatment removes the confounding phosphorylation allowing the accurate quantification of CaMKIIα ubiquitination at K291, independent of its phosphorylation status. *D*, representative extracted fragment ion chromatograms for endogenous/"light" and standard/"heavy" CaMKIIα peptide (QETVDCLKK) ubiquitinated at K291, and its doubly modified variant bearing ubiquitination at K291 and phosphorylation at T286, before and after QuickCIP treatment. The different colors represent distinct fragments b and y ions of the indicated peptide. *E*, summary barplot showing the mean light-to-heavy peak area ratios. Limma statistical testing was performed to determine significant differences and account for the synaptosome preparation batch effect (N = six independent stimulation experiments, with 2 MS measurement replicates for each experiment). *$p < 0.05$, ***$p < 0.001$. We note that for the sake of simplicity, we show here only one synaptosome preparation batch with three independent stimulation experiments. For a detailed view of both synaptosome batches refer to supplemental Fig. S5.

Ca^{2+} influx in depolarized synaptosomes. Given the fast response, the location, and the conservation of this site, we hypothesized that (de)ubiquitination might be involved in regulating CaMKIIα activity.

First, we investigated whether CaMKIIα stably expressed in HeLa cells can be used to assess the effect of K291 ubiquitination on CaMKIIα activity (Fig. 5*B*), while also monitoring the quantitative changes of ubiquitination at K291 and

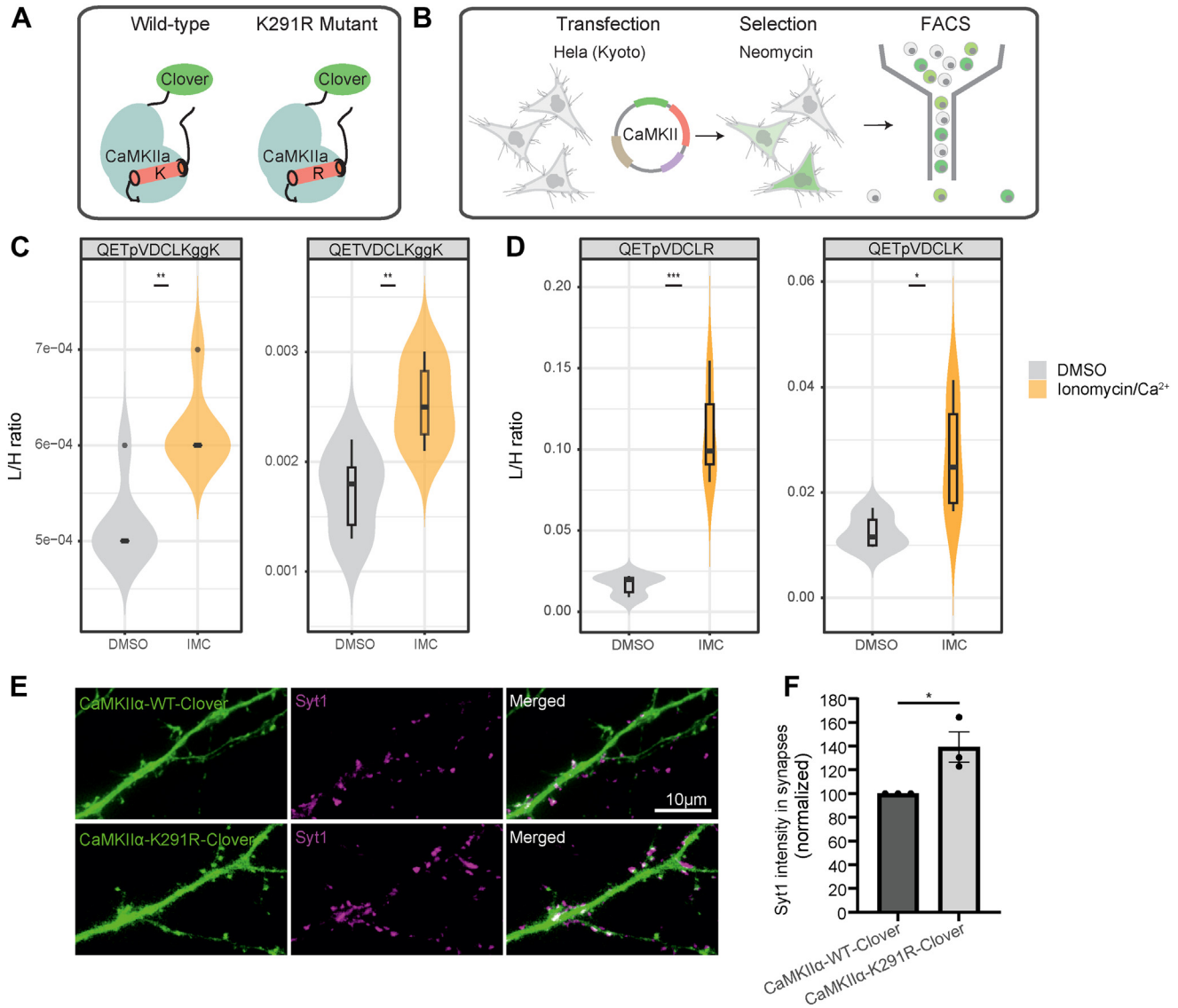

FIG. 5. **Functional assay to monitor the effects of CaMKIIα expression in HeLa cells and neurons.** *A*, generation of CaMKIIα K291R mutant that cannot be ubiquitinated at K291. *B*, generation of HeLa Kyoto cell lines stably expressing either CaMKIIα-WT or the mutant variant K291R. *C* and *D*, Violin plots illustrating the endogenous/"light"-to-standard/"heavy" peptide intensities in HeLa cells under different conditions (Ionomycin/Ca^{2+}-vs-DMSO). We note that we used the same standard/"heavy" peptide with the sequence QETpVDCLK to normalize the endogenous/light peptides QETpVDCLK and QETpVDCLR. A two-sample *t* test was performed to determine significant differences (N = three independent stimulation experiments, with 2 MS measurement replicates for each experiment). *$p < 0.05$, ***$p < 0.001$. *E*, neurons were transfected with either the wild type (WT) or the K291R variants of CaMKIIα and were analyzed by fluorescence microscopy 6 to 8 days later. The green channel indicates the CaMKIIα expression, while the magenta channel shows anti-synaptotagmin 1 antibodies (directly conjugated to the fluorophore Atto647N), which are taken up by recycling synaptic vesicles, during a 60-min incubation. After washing with Tyrode's solution, the cells were fixed with PFA and imaged. *F*, synapses were identified based on the synaptotagmin 1 signal, which was correlated with the CaMKIIα expression signal within the area of each synapse, using a Pearson correlation analysis. Subsequently, the fluorescence intensity of the synaptotagmin 1 label was quantified in the boutons in which the two signals were well correlated (meaning true presynaptic boutons, and not presynapses of non-transfected neurons that overlapped with CaMKIIα-expressing dendrites). A paired *t* test between the wild type and the mutant was performed to determine significant differences ($p = 0.03$, N = three independent experiments, with hundreds of synapses analysed for each experiment).

autophosphorylation at T286 in response to Ca^{2+}- influx using PRM-MS (supplemental Tables S6, supplemental Data 3.5, and 3.6). Ca^{2+} influx was induced by treating HeLa cells with the Ca^{2+} ionophore, ionomycin, and 1.8 mM of Ca^{2+} for 7 min. As expected, we observed an increase in T286 autophosphorylation upon stimulation (Fig. 5*D* and supplemental Data S6), indicative of CaMKIIα activation. In addition, we observed an increase in K291 ubiquitination on singly

modified peptides and doubly modified ones, bearing both phosphorylation at T286 and ubiquitination at K291 (Fig. 5*C* and supplemental Data S6). Together, these PRM data show that CaMKIIα undergoes phosphorylation and ubiquitination on T286 and K291, respectively, also in non-neuronal cells. However, we observe opposing changes in its ubiquitination state in the two systems we studied; whereas CaMKIIα undergoes deubiquitination at K291 in response to Ca^{2+} influx in synaptosomes, the fluorescence-labeled CaMKIIα undergoes ubiquitination at K291 upon Ca^{2+} stimulation in HeLa cells.

Despite this difference, we investigated the effect of the ubiquitination-deficient variant in the HeLa cells in response to ionomycin treatment, monitoring Ca^{2+}-induced differences in T286 autophosphorylation compared to the wild type by PRM-MS. Strikingly, we observed that the K291R variant displayed significantly increased levels of T286 phosphorylation compared to the wild type (Fig. 5*D* and supplemental Data S6). This reveals that the absence of ubiquitination at K291 significantly increases the level of T286 for autophosphorylation, indicative of higher CaMKIIα activity.

In isolated synapses, CaMKII activity has been shown to correlate with synaptic activity, with high CaMKII activity being associated with increased rates of neurotransmitter release (65). Therefore, we hypothesized that an increase in activity of the mutated, non-ubiquitinated CaMKIIα may lead to an increased increased exocytosis of synaptic vesicles (SVs) and neurotransmitter release. To investigate this idea, we expressed the wild type and the K291R variant in cultured hippocampal neurons. We probed the neurons with an antibody directed against the lumenal (intravesicular) domain of synaptotagmin 1, which is taken up by recycling SVs and therefore provides an overall view of the changes in exocytosis and synaptic activity levels (66). We observed that synaptic boutons in the neurons expressing the K291R variant showed significantly higher synaptotagmin 1 labeling, which reflects an enhanced activity in exocytosis (Fig. 5, *E* and *F*). As CaMKIIα activity correlates with exocytosis/neurotransmitter release, these results corroborate our hypothesis that the (de) ubiquitination at K291 influences CaMKIIα activity.

DISCUSSION

In this study, we used a quantitative proteomics strategy to characterize ubiquitination changes of synaptosomal proteins that occur upon Ca^{2+} influx in isolated nerve terminals. We generated an inventory of ubiquitination sites mapped to proteins in the synapse. 65% of the sites we identified were previously reported in the PhosphositePlus database (48), but not specifically for the synapse; 35% have not been reported before. Our inventory thus provides a rich resource for the neuroscience community, with many new ubiquitination sites that can be further analyzed functionally, *e.g.*, interrogating their effects on protein–protein interaction relevant to SV exocytosis, endocytosis, and recycling during depolarization in the synapse. For instance, we have identified multiple novel ubiquitination sites in the active zone protein RIM1, a known substrate of ubiquitination (22). Interestingly, all four ubiquitination sites were mapped to the C-terminus of RIM1, a region known to interact with the substrate recognition subunit SCRAPPER(or *Fbxl20*) of the SKP1-CUL1-F-box E3 ligase (22). In addition, our dataset includes ubiquitination sites on 11 E3 ligases and 29 DUBs, potentially representing the E3 ligases and DUBs that may be particularly relevant in the synapse (detailed list in supplemental Tables S7 and S8).

Several conclusions can be drawn from our quantitative analysis of ubiquitination sites in depolarized synaptosomes under Ca^{2+}-rich and Ca^{2+}-depleted conditions. First, compared to protein phosphorylation, for which substantial changes were observed in the phosphoproteome (13), a rather small fraction of proteins and their respective ubiquitination sites changed significantly 2 min after depolarization. It is possible that ubiquitination changes critical for regulating long-term synaptic processes (21–23, 67, 68) unfold over extended periods, and the changes observed here represent early responses. Furthermore, these limited changes in ubiquitination may result from the intrinsic specificity of the ubiquitination process, which relies on the high substrate selectivity of E3 ubiquitin ligases. Specific stimuli are likely to activate E3 ligases, leading to the targeted ubiquitination of select proteins, as demonstrated for the neuronal E3 ligase Nedd4-1 (69, 70). Notably, among the regulated ubiquitination sites, those that were upregulated during Ca^{2+} influx were mapped to the active-zone proteins, Cadps1, Munc-18, and Syt-7. In contrast, de-ubiquitination upon depolarization was observed for particular sites in proteins involved in clathrin-mediated endocytosis (CME), namely AP180, EPS15L, and Pip5k1c. Stimulation-dependent deubiquitination of certain CME proteins, epsin-1 and EPS15, has been observed before in depolarized synaptosomes using immunoblotting (26). Although our study shows a similar effect on the ubiquitination state of CME proteins, we did not monitor the deubiquitination of epsin-1 and ESP15, which may be attributed to the different stimulation times used in our study.

The deubiquitination of CME proteins is of particular interest, as it coincides with their dephosphorylation that was previously observed in response to stimulation (10, 11). Among the CME proteins observed to be dephosphorylated and deubiquitinated in response to stimulation, we detected the clathrin adaptor protein AP180. Dephosphorylation of AP180, which is known to take place in depolarized synaptosomes (13), promotes its interaction with the AP-2 adaptor complex that is necessary for SV endocytosis (71). In this study, we report that, upon stimulation, AP180 undergoes stark deubiquitination at K28, which is located in the N-terminal ANTH domain known to bind to plasma-membrane regions containing phosphatidiylinositol-4,5-biphosphate ($PI(4,5)P_2$) (55, 72). Specifically, K28 of the ANTH domain was shown to interact with the 5-phosphate of $PI(4,5)P_2$, together

with two other lysine residues (K38, K40) and a histidine residue (H41) (72). We hypothesize that under resting conditions the ANTH domain is ubiquitinated at K28, which attenuates its interaction with $PI(4,5)P_2$-containing regions. Upon stimulation, AP180 undergoes deubiquitination at K28, resulting in its recruitment of AP180 to those regions where it can perform clathrin-adaptor functions. We propose that stimulation-dependent deubiquitination of AP180 allows its recruitment to endocytic regions, consistent with an increased rate of endocytosis in depolarized synaptosomes. Further investigation is required to establish the role of K28 ubiquitination in regulating the localization of the adaptor-clathrin protein AP180 and thus the rate of clathrin-mediated endocytosis. As the regulated ubiquitination and phosphorylation sites of AP180 do not reside within the same tryptic peptide, it is also unclear whether the modifications affect the same protein molecule.

In CaMKIIα, the regulated ubiquitination site (K291) was mapped to the autoinhibitory domain spanning the amino acid 274 to 314. This domain is subject to a number of other post-translational modifications (PTMs), including T286 autophosphorylation, S280 O-linked glycosylation, and M281/282 oxidation (62, 63, 73, 74). In particular autophosphorylation at T286 occurs after Ca^{2+}/calmodulin-dependent activation of CaMKIIα, rendering CaMKIIα Ca^{2+}-independent (62, 63). Similar to T286 autophosphorylation, other reported PTMs in the regulatory domain (64, 73–75) occur after its Ca^{2+}-triggered activation and render CaMKIIα Ca^{2+}-independent. Our quantitative ubiquitinomic study revealed strong deubiquitination at K291 of CaMKIIα in synaptosomes. Importantly, this deubiquination is accompanied by a stark phosphorylation at T286 upon Ca^{2+} influx, with both modifications co-occurring within the same peptide and hence in the same protein. This provides an intriguing example of the tight crosstalk of phosphorylation and ubiquitination, a regulatory paradigm in eukaryotic cell biology. Given that both post-translational modifications occur within the same tryptic peptide, the well-documented stimulation-triggered T286 phosphorylation likely converts the singly ubiquitinated form of CaMKIIα into a phosphorylated-ubiquitinated form. This conversion could account for the observed decrease in the levels of singly ubiquitinated form at K291. Two possible mechanisms could explain this observation (1): the decrease is entirely due to the conversion of ubiquitinated CaMKIIα to the phosphorylated-ubiquitinated form during stimulation, or (2) active deubiquitination at K291 occurs during stimulation, or (3) a combination of both processes. Through absolute quantification and experiments eliminating T286 autophosphorylation, we demonstrated that both mechanisms are at play.

In contrast to depolarized synaptosomes, our PRM-MS in HeLa cell culture expressing a CaMKIIα chimeric protein revealed an increase in K291 ubiquitination of CaMKIIα in response to Ca^{2+} influx. However, the apparent discrepancy between the HeLa cell and synaptosome findings likely arises from the differences in cellular context and CaMKIIα functionality. In HeLa cells, CaMKIIα is overexpressed and presumably serves no function there, which may result in ubiquitination kinetics that differ from those observed in synapses, where CaMKIIα activity is tightly regulated and functionally relevant. HeLa cells were used here to specifically assess the effects of CaMKIIα mutants on T286 autophosphorylation. Importantly, a Lys-to-Arg substitution at residue 291 resulted in elevated levels of T286 autophosphorylation upon Ca^{2+} influx, suggesting enhanced CaMKIIα activity. In line with this finding, the expression of the non-ubiquitinated K291R variant in primary neurons resulted in enhanced synaptic activity compared to the wild-type form.

K291R point mutation is located in the autoinhibitory domain of CaMKIIα and could theoretically influence enzyme activity independent of its ubiquitination status, through one of three mechanisms: (a) participating in intramolecular interactions between the autoinhibitory domain and the active site of the enzyme, to maintain it in the close, inactive state, (b) affecting calmodulin (CaM) binding to the CaM-binding domain, or (c) influencing T286 substrate recognition for autophosphorylation, *in trans*. However, structural evidence suggests that K291 is solvent-exposed in the autoinhibitory state and does not appear to play a role in stabilizing the closed, inactive conformation (supplemental Fig. S6) (76–79). Similarly, the available structure of the CaMKIIα-CaM complex indicates that K291 residue does not interact with CaM in the open/active state (78) and is not part of the core CaM-binding domain (80) (supplemental Fig. S6), making the second mechanism less likely. Nevertheless, K291 may play a role in the conformational transition between the closed and open states. Finally, structural evidence suggests that K291 does not directly participate in substrate recognition (78).

Alternatively, ubiquitination at K291 ubiquitination could directly impact CaMKIIα activity through one of the following mechanisms. First, K291 ubiquitination could result in dislodging the autoinhibitory segment, thus activating CaMKIIα. Once activated and in the open conformation, CaMKIIα subunits within the holoenzyme could undergo autophosphorylation in trans at T286 by neighboring subunits, enhancing CaMKIIα activation. Conversely, K291 ubiquitination could inhibit CaMKIIα activity through steric constraints that interfere with CaM binding or T286 autophosphorylation, given that ubiquitin is a large post-translational modification. In line with the latter hypothesis, we observed deubiquitination along with increased autophosphorylation in the regulatory domain of CaMKIIα upon Ca^{2+} influx in isolated synaptosomes. Together these findings highlight the functional importance of K291 ubiquitination and provide further support for the non-degradative roles of CaMKIIα ubiquitination. However, our proteomic data do not allow us to directly determine whether CaMKIIα is mono- or polyubiquitinated at K291.

Previous studies have shown the regulation of kinase activities by intermolecular interactions with poly-ubiquitin

chains (81–83). For instance, in the canonical NFκB signaling pathway, two kinases, TAK1 and IKK, undergo activation by interactions with K63-linked or K63/M1-linked ubiquitin chains (68, 69, 71). However, the direct conjugation of ubiquitin to kinases, which serves non-degradative roles remains poorly understood (84). In this context, our study illustrates an emerging, additional facet of ubiquitin-mediated regulation through the direct conjugation of ubiquitin to a kinase.

DATA AVAILABILITY

The mass spectrometry data have been deposited to the ProteomeXchange Consortium *via* the PRIDE (85) partner repository with the data set identifier PXD052826. Reviewer access details. Project accession: PXD052826. Token: Gk734PlQcYgo Alternatively, reviewer can access the dataset by logging in to the PRIDE website using the following account details: Username: reviewer_pxd052826@ebi.ac.uk. Password: 6wqGr998HQn3.

Additionally, the Skyline analysis files have been deposited to Panorama Public (doi: https://doi.org/10.6069/ktev-hs45) with the data set identifier PXD053470. Reviewer account details. Email: panorama+reviewer274@proteinms.net. Password: pe@?+%!bO$rF9.

Supplemental data—This article contains supplemental data (13, 43–45, 76–79, 86).

Acknowledgments—We thank Reinhard Jahn for his support in this study. We further thank the Facility of Light Microscopy, and especially Peter Lenart, Antonio Politi and Jasmin Jakobi for their assistance in HeLa cell culture, FACS (fluorescence-activated cell sorting) and live imaging. We further acknowledge Ralf Pflanz, Monika Raabe, Uwe Plessmann, Olexandr Dybkov and Sabine König for help with MS, as well as Sascha Krause, Thomas Gundlach and Ulrike Teichmann for their assistance in animal experiments.

Funding and additional information—H. U, S. O. R. were funded by the Deutsche Forschungsgemeinschaft and the collaborative research center SFB1286 (project numbers A08 and A03). S. L. was funded by Deutsche Forschungsgemeinschaft and the collaborative research center SFB1565 (project number P17).

Author contributions—I. S., S. A., S. O. R., H. U., S. V. G., and S. L. writing–review & editing; I. S., S. A., S. O. R., H. U., S. V. G., and S. K. investigation; I. S., S. A., S. O. R., H. U., S. V. G., and S. K. formal analysis; I. S., S. A., H. U., and S. L. conceptualization. S. A. and H. U. writing–original draft; S. A. and H. U. visualization; S. A. and H. U. validation; S. A. and H. U. software; S. A. and H. U. resources; S. A. and H. U. project administration; S. A., H. U., S. V. G., S. L., and S. K. methodology; S. A. and H. U. data curation. S. O. R. and H. U. supervision, S. O. R., H. U., and S. L. funding acquisition.

Conflict of interest—The authors state that they have no conflicts of interest with the contents of the article.

Abbreviations—The abbreviations used are: ACN, acetonitrile; AGC, Automatic gain control; ANTH, AP180 N-terminal homology; AP180, adaptor protein 180; AZ, active zone; bRP, basic reversed-phase; BSA, Bovine serum albumin; CAA, Chloroacetamide; CaMKII, Ca^{2+}/calmodulin-dependent kinase II; CME, clathrin-mediated endocytosis; DUB, deubiquitinase; E1, ubiquitin-activating enzyme; E2, ubiquitin-conjugating enzyme; E3, ubiquitin-ligase enzyme; ELKS, protein rich in the amino acids E, L, K, and S; Eps15, epidermal growth factor receptor substrate 15; EPS15L, epidermal growth factor receptor substrate 15-like; FA, formic acid; FBS, Fetal bovine serum; FDR, false discovery rate; GA, Glycolic acid; GluDH, Glutamic dehydrogenase; K-ε-GG, Ubiquitin remnant diglycine dipeptide; LC-MS/MS, liquid chromatography - tandem mass spectrometry; MS, mass spectrometry; MQ, MaxQuant; NCE, Normalized collision energy; NT, neurotransmitter; Pclo, Piccolo; $PI(4,5)P_2$, phosphatidylinositol-4,5 biphosphate; Pip5k1c, Phosphatidylinositol 4-phosphate 5-kinase type-1 gamma; PRM, parallel reaction monitoring; PSM, peptide-spectrum match; PTM, post-translational modification; RIM, Rab-3 interacting molecule; RIM-BP, RIM-binding protein; RP, Reverse pool; RRP, readily releasable pool; SV, synaptic vesicle; Syt1, Synaptotagmin-1; Syt7, Synaptotagmin-7; Stx1, Syntaxin-1; TAK1, TGF-β-activated kinase 1; TCEP, Tris(2-carboxylethyl)phosphine; TMT, tandem mass tags; UPS, ubiquitin-proteasome system.

Received September 6, 2024, and in revised form, January 29, 2025
Published, MCPRO Papers in Press, March 13, 2025, https://doi.org/10.1016/j.mcpro.2025.100946

REFERENCES

1. Denker. (2010) Synaptic vesicle pools: an update. *Front. Synaptic Neurosci.* **2**, 135
2. Südhof, T. C. (2012) The presynaptic active zone. *Neuron* **75**, 11–25
3. Jahn, R., and Fasshauer, D. (2012) Molecular machines governing exocytosis of synaptic vesicles. *Nature* **490**, 201–207
4. Sudhof, T. C. (2012) Calcium control of neurotransmitter release. *Cold Spring Harb. Perspect. Biol.* **4**, a011353
5. Toonen, R. F. G., and Verhage, M. (2007) Munc18-1 in secretion: lonely Munc joins SNARE team and takes control. *Trends Neurosci.* **30**, 564–572
6. Chanaday, N. L., Cousin, M. A., Milosevic, I., Watanabe, S., and Morgan, J. R. (2019) The synaptic vesicle cycle revisited: new insights into the modes and mechanisms. *J. Neurosci.* **39**, 8209–8216
7. Greengard, P., Benfenati, F., and Valtorta, F. (1994) Synapsin I, an actin-binding protein regulating synaptic vesicle traffic in the nerve terminal. *Adv. Second Messenger Phosphoprotein Res.* **29**, 31–45
8. Ceccaldi, P. E., Grohovaz, F., Benfenati, F., Chieregatti, E., Greengard, P., and Valtorta, F. (1995) Dephosphorylated synapsin I anchors synaptic vesicles to actin cytoskeleton: an analysis by videomicroscopy. *J. Cell Biol.* **128**, 905–912
9. Cesca, F., Baldelli, P., Valtorta, F., and Benfenati, F. (2010) The synapsins: key actors of synapse function and plasticity. *Prog. Neurobiol.* **91**, 313–348
10. Cousin, M. A., and Robinson, P. J. (2001) The dephosphins: dephosphorylation by calcineurin triggers synaptic vesicle endocytosis. *Trends Neurosci.* **24**, 659–665

11. Kohansal-Nodehi, M., Chua, J. J., Urlaub, H., Jahn, R., and Czernik, D. (2016) Analysis of protein phosphorylation in nerve terminal reveals extensive changes in active zone proteins upon exocytosis. *eLife* **5**, e14530
12. Engholm-Keller, K., Waardenberg, A. J., Müller, J. A., Wark, J. R., Fernando, R. N., Arthur, J. W., *et al*. (2019) The temporal profile of activity-dependent presynaptic phospho-signalling reveals long-lasting patterns of poststimulus regulation. *PLoS Biol.* **17**, e3000170
13. Silbern, I., Pan, K.-T., Fiosins, M., Bonn, S., Rizzoli, S. O., Fornasiero, E. F., *et al*. (2021) Protein phosphorylation in depolarized synaptosomes: dissecting primary effects of calcium from synaptic vesicle cycling. *Mol. Cell Proteomics* **20**, 100061
14. Kwon, Y. T., and Ciechanover, A. (2017) The ubiquitin code in the ubiquitin-proteasome system and autophagy. *Trends Biochem. Sci.* **42**, 873–886
15. Sarraf, S. A., Raman, M., Guarani-Pereira, V., Sowa, M. E., Huttlin, E. L., Gygi, S. P., *et al*. (2013) Landscape of the PARKIN-dependent ubiquitylome in response to mitochondrial depolarization. *Nature* **496**, 372–376
16. Raiborg, C., and Stenmark, H. (2009) The ESCRT machinery in endosomal sorting of ubiquitylated membrane proteins. *Nature* **458**, 445–452
17. Chin, L.-S., Vavalle, J. P., and Li, L. (2002) Staring, a novel E3 ubiquitin-protein ligase that targets syntaxin 1 for degradation. *J. Biol. Chem.* **277**, 35071–35079
18. Wheeler, T. C., Chin, L.-S., Li, Y., Roudabush, F. L., and Li, L. (2002) Regulation of synaptophysin degradation by mammalian homologues of seven in absentia. *J. Biol. Chem.* **277**, 10273–10282
19. van Roessel, P., Elliott, D. A., Robinson, I. M., Prokop, A., and Brand, A. H. (2004) Independent regulation of synaptic size and activity by the anaphase-promoting complex. *Cell* **119**, 707–718
20. Speese, S. D., Trotta, N., Rodesch, C. K., Aravamudan, B., and Broadie, K. (2003) The ubiquitin proteasome system acutely regulates presynaptic protein turnover and synaptic efficacy. *Curr. Biol.* **13**, 899–910
21. Lazarevic, V., Schone, C., Heine, M., Gundelfinger, E. D., and Fejtova, A. (2011) Extensive remodeling of the presynaptic cytomatrix upon homeostatic adaptation to network activity silencing. *J. Neurosci.* **31**, 10189–10200
22. Yao, I., Takagi, H., Ageta, H., Kahyo, T., Sato, S., Hatanaka, K., *et al*. (2007) SCRAPPER-dependent ubiquitination of active zone protein RIM1 regulates synaptic vesicle release. *Cell* **130**, 943–957
23. Jiang, X., Litkowski, P. E., Taylor, A. A., Lin, Y., Snider, B. J., and Moulder, K. L. (2010) A role for the ubiquitin–proteasome system in activity-dependent presynaptic silencing. *J. Neurosci.* **30**, 1798–1809
24. Waites, C. L., Leal-Ortiz, S. A., Okerlund, N., Dalke, H., Fejtova, A., Altrock, W. D., *et al*. (2013) Bassoon and Piccolo maintain synapse integrity by regulating protein ubiquitination and degradation. *EMBO J.* **32**, 954–969
25. Rinetti, G. V., and Schweizer, F. E. (2010) Ubiquitination acutely regulates presynaptic neurotransmitter release in mammalian neurons. *J. Neurosci.* **30**, 3157–3166
26. Chen, H., Polo, S., Di Fiore, P. P., and De Camilli, P. V. (2003) Rapid Ca^{2+}-dependent decrease of protein ubiquitination at synapses. *Proc. Natl. Acad. Sci. U. S. A.* **100**, 14908–14913
27. Xu, G., Paige, J. S., and Jaffrey, S. R. (2010) Global analysis of lysine ubiquitination by ubiquitin remnant immunoaffinity profiling. *Nat. Biotechnol.* **28**, 868–873
28. Kim, W., Bennett, E. J., Huttlin, E. L., Guo, A., Li, J., Possemato, A., *et al*. (2011) Systematic and quantitative assessment of the ubiquitin-modified proteome. *Mol. Cell* **44**, 325–340
29. Wagner, S. A., Beli, P., Weinert, B. T., Nielsen, M. L., Cox, J., Mann, M., *et al*. (2011) A proteome-wide, quantitative survey of *in vivo* ubiquitylation sites reveals widespread regulatory roles. *Mol. Cell Proteomics* **10**. https://doi.org/10.1074/mcp.M111.013284
30. Povlsen, L. K., Beli, P., Wagner, S. A., Poulsen, S. L., Sylvestersen, K. B., Poulsen, J. W., *et al*. (2012) Systems-wide analysis of ubiquitylation dynamics reveals a key role for PAF15 ubiquitylation in DNA-damage bypass. *Nat. Cell Biol.* **14**, 1089–1098
31. Satpathy, S., Wagner, S. A., Beli, P., Gupta, R., Kristiansen, T. A., Malinova, D., *et al*. (2015) Systems-wide analysis of BCR signalosomes and downstream phosphorylation and ubiquitylation. *Mol. Syst. Biol.* **11**, 810
32. Udeshi, N. D., Mani, D. C., Satpathy, S., Fereshetian, S., Gasser, J. A., Svinkina, T., *et al*. (2020) Rapid and deep-scale ubiquitylation profiling for biology and translational research. *Nat. Commun.* **11**, 359
33. Hansen, F. M., Tanzer, M. C., Brüning, F., Bludau, I., Stafford, C., Schulman, B. A., *et al*. (2021) Data-independent acquisition method for ubiquitinome analysis reveals regulation of circadian biology. *Nat. Commun.* **12**, 254
34. Na, C. H., Jones, D. R., Yang, Y., Wang, X., Xu, Y., and Peng, J. (2012) Synaptic protein ubiquitination in rat brain revealed by antibody-based ubiquitome analysis. *J. Proteome Res.* **11**, 4722–4732
35. Wagner, S. A., Beli, P., Weinert, B. T., Schölz, C., Kelstrup, C. D., Young, C., *et al*. (2012) Proteomic analyses reveal divergent ubiquitylation site patterns in murine tissues. *Mol. Cell Proteomics* **11**, 1578–1585
36. Gray, E. G., and Whittaker, V. P. (1962) The isolation of nerve endings from brain: an electron-microscopic study of cell fragments derived by homogenization and centrifugation. *J. Anat.* **96**, 79–88
37. Nicholls, D. G., Sihra, T. S., and Sanchez-Prieto, J. (1987) Calcium-dependent and-independent release of glutamate from synaptosomes monitored by continuous Fluorometry. *J. Neurochem.* **49**, 50–57
38. Thompson, A., Schäfer, J., Kuhn, K., Kienle, S., Schwarz, J., Schmidt, G., *et al*. (2003) Tandem mass tags: a novel quantification strategy for comparative analysis of complex protein mixtures by MS/MS. *Anal. Chem.* **75**, 1895–1904
39. von Mollard, G. F., Südhof, T. C., and Jahn, R. (1991) A small GTP-binding protein dissociates from synaptic vesicles during exocytosis. *Nature* **349**, 79–81
40. Nicholls, D. G., and Sihra, T. S. (1986) Synaptosomes possess an exocytotic pool of glutamate. *Nature* **321**, 772–773
41. Wessel, D., and Flügge, U. I. (1984) A method for the quantitative recovery of protein in dilute solution in the presence of detergents and lipids. *Anal. Biochem.* **138**, 141–143
42. Udeshi, N. D., Mertins, P., Svinkina, T., and Carr, S. A. (2013) Large-scale identification of ubiquitination sites by mass spectrometry. *Nat. Protoc.* **8**, 1950–1960
43. Cox, J., Neuhauser, N., Michalski, A., Scheltema, R. A., Olsen, J. V., and Mann, M. (2011) Andromeda: a peptide search engine integrated into the MaxQuant environment. *J. Proteome Res.* **10**, 1794–1805
44. Tyanova, S., Temu, T., and Cox, J. (2016) The MaxQuant computational platform for mass spectrometry-based shotgun proteomics. *Nat. Protoc.* **11**, 2301–2319
45. The UniProt Consortium. (2019) UniProt: a worldwide hub of protein knowledge. *Nucleic Acids Res.* **47**, D506–D515
46. Ritchie, M. E., Phipson, B., Wu, D., Hu, Y., Law, C. W., Shi, W., *et al*. (2015) Limma powers differential expression analyses for RNA-sequencing and microarray studies. *Nucleic Acids Res.* **43**, e47
47. Koopmans, F., van Nierop, P., Andres-Alonso, M., Byrnes, A., Cijsouw, T., Coba, M. P., *et al*. (2019) SynGO: an evidence-based, expert-curated knowledge base for the synapse. *Neuron* **103**, 217–234.e4
48. Hornbeck, P. V., Zhang, B., Murray, B., Kornhauser, J. M., Latham, V., and Skrzypek, E. (2015) PhosphoSitePlus, 2014: mutations, PTMs and recalibrations. *Nucleic Acids Res.* **43**, D512–D520
49. Altschul, S. F., Gish, W., Miller, W., Myers, E. W., and Lipman, D. J. (1990) Basic local alignment search tool. *J. Mol. Biol.* **215**, 403–410
50. MacLean, B., Tomazela, D. M., Shulman, N., Chambers, M., Finney, G. L., Frewen, B., *et al*. (2010) Skyline: an open source document editor for creating and analyzing targeted proteomics experiments. *Bioinformatics* **26**, 966–968
51. Storey, J. D., and Tibshirani, R. (2003) Statistical significance for genome-wide studies. *Proc. Natl. Acad. Sci. U. S. A.* **100**, 9440–9445
52. Moggridge, S, Sorensen, P. H., Morin, G. B., and Hughes, C. S. (2018) Extending the compatibility of the SP3 paramagnetic bead processing approach for proteomics. *J. Proteome Res.* **17**, 1730–1740
53. Kaech, S., and Banker, G. (2006) Culturing hippocampal neurons. *Nat. Protoc.* **1**, 2406–2415
54. Ge, S. X., Jung, D., and Yao, R. (2020) ShinyGO: a graphical gene-set enrichment tool for animals and plants. *Bioinformatics* **36**, 2628–2629
55. Stahelin, R. V., Long, F., Peter, B. J., Murray, D., De Camilli, P., McMahon, H. T., *et al*. (2003) Contrasting membrane interaction mechanisms of AP180 N-terminal homology (ANTH) and epsin N-terminal homology (ENTH) domains. *J. Biol. Chem.* **278**, 28993–28999
56. De Camilli, P., Chen, H., Hyman, J., Panepucci, E., Bateman, A., and Brunger, A. T. (2002) The ENTH domain. *FEBS Lett.* **513**, 11–18
57. Peterson, A. C., Russell, J. D., Bailey, D. J., Westphall, M. S., and Coon, J. J. (2012) Parallel reaction monitoring for high resolution and high mass

accuracy quantitative, targeted proteomics. *Mol. Cell Proteomics* **11**, 1475–1488
58. Ting, L., Rad, R., Gygi, S. P., and Haas, W. (2011) MS3 eliminates ratio distortion in isobaric multiplexed quantitative proteomics. *Nat. Methods* **8**, 937–940
59. Fornasiero, E. F., Mandad, S., Wildhagen, H., Alevra, M., Rammner, B., Keihani, S., *et al*. (2018) Precisely measured protein lifetimes in the mouse brain reveal differences across tissues and subcellular fractions. *Nat. Commun.* **9**, 4230
60. Payne, M. E., Fong, Y. L., Ono, T., Colbran, R. J., Kemp, B. E., Soderling, T. R., *et al*. (1988) Calcium/calmodulin-dependent protein kinase II. Characterization of distinct calmodulin binding and inhibitory domains. *J. Biol. Chem.* **263**, 7190–7195
61. Colbran, R. J., Fong, Y. L., Schworer, C. M., and Soderling, T. R. (1988) Regulatory interactions of the calmodulin-binding, inhibitory, and autophosphorylation domains of Ca2+/calmodulin-dependent protein kinase II. *J. Biol. Chem.* **263**, 18145–18151
62. Thiel, G., Czernik, A. J., Gorelick, F., Nairn, A. C., and Greengard, P. (1988) Ca2+/calmodulin-dependent protein kinase II: identification of threonine-286 as the autophosphorylation site in the alpha subunit associated with the generation of Ca2+-independent activity. *Proc. Natl. Acad. Sci. U. S. A.* **85**, 6337–6341
63. Schworer, C. M., Colbran, R. J., Keefer, J. R., and Soderling, T. R. (1988) Ca2+/calmodulin-dependent protein kinase II. Identification of a regulatory autophosphorylation site adjacent to the inhibitory and calmodulin-binding domains. *J. Biol. Chem.* **263**, 13486–13489
64. Hanson, P. I., Meyer, T., Stryer, L., and Schulman, H. (1994) Dual role of calmodulin in autophosphorylation of multifunctional cam kinase may underlie decoding of calcium signals. *Neuron* **12**, 943–956
65. Nichols, R. A., Sihra, T. S., Czernik, A. J., Nairn, A. C., and Greengard, P. (1990) Calcium/calmodulin-dependent protein kinase II increases glutamate and noradrenaline release from synaptosomes. *Nature* **343**, 647–651
66. Matteoli, M., Takei, K., Perin, M., Südhof, T., and De Camilli, P. (1992) Exo-endocytotic recycling of synaptic vesicles in developing processes of cultured hippocampal neurons. *J. Cell Biol.* **117**, 849–861
67. Wilson, S. M., Bhattacharyya, B., Rachel, R. A., Coppola, V., Tessarollo, L., Householder, D. B., *et al*. (2002) Synaptic defects in ataxia mice result from a mutation in Usp14, encoding a ubiquitin-specific protease. *Nat. Genet.* **32**, 420–425
68. Walters, B. J., Hallengren, J. J., Theile, C. S., Ploegh, H. L., Wilson, S. M., and Dobrunz, L. E. (2014) A catalytic independent function of the deubiquitinating enzyme USP14 regulates hippocampal synaptic short-term plasticity and vesicle number. *J. Physiol.* **592**, 571–586
69. Schwarz, L. A., Hall, B. J., and Patrick, G. N. (2010) Activity-dependent ubiquitination of GluA1 mediates a distinct AMPA receptor endocytosis and sorting pathway. *J. Neurosci.* **30**, 16718–16729
70. Scudder, S. L., Goo, M. S., Cartier, A. E., Molteni, A., Schwarz, L. A., Wright, R., *et al*. (2014) Synaptic strength is bidirectionally controlled by opposing activity-dependent regulation of nedd4-1 and USP8. *J. Neurosci.* **34**, 16637–16649
71. Hao, W., Luo, Z., Zheng, L., Prasad, K., and Lafer, E. M. (1999) AP180 and AP-2 interact directly in a complex that cooperatively assembles clathrin. *J. Biol. Chem.* **274**, 22785–22794
72. Ford, M. G. J., Pearse, B. M. F., Higgins, M. K., Vallis, Y., Owen, D. J., Gibson, A., *et al*. (2001) Simultaneous binding of PtdIns(4,5)P_2 and clathrin by AP180 in the nucleation of clathrin lattices on membranes. *Science* **291**, 1051–1055
73. Erickson, J. R., Joiner, M. A., Guan, X., Kutschke, W., Yang, J., Oddis, C. V., *et al*. (2008) A dynamic pathway for calcium-independent activation of CaMKII by methionine oxidation. *Cell* **133**, 462–474
74. Erickson, J. R., Pereira, L., Wang, L., Han, G., Ferguson, A., Dao, K., *et al*. (2013) Diabetic hyperglycaemia activates CaMKII and arrhythmias by O-linked glycosylation. *Nature* **502**, 372–376
75. Erickson, J. R., Patel, R., Ferguson, A., Bossuyt, J., and Bers, D. M. (2011) Fluorescence resonance energy transfer–based sensor camui provides new insight into mechanisms of calcium/calmodulin-dependent protein kinase II activation in intact cardiomyocytes. *Circ. Res.* **109**, 729–738
76. Chao, L. H., Stratton, M. M., Lee, I.-H., Rosenberg, O. S., Levitz, J., Mandell, D. J., *et al*. (2011) A mechanism for tunable autoinhibition in the structure of a human Ca2+/calmodulin- dependent kinase II holoenzyme. *Cell* **146**, 732–745
77. Myers, J. B., Zaegel, V., Coultrap, S. J., Miller, A. P., Bayer, K. U., and Reichow, S. L. (2017) The CaMKII holoenzyme structure in activation-competent conformations. *Nat. Commun.* **8**, 15742
78. Rellos, P., Pike, A. C. W., Niesen, F. H., Salah, E., Lee, W. H., Delft, F., *et al*. (2010) Structure of the CaMKIIδ/calmodulin complex reveals the molecular mechanism of CaMKII kinase activation. *PLoS Biol.* **8**, e1000426
79. Rosenberg, O. S., Deindl, S., Sung, R.-J., Nairn, A. C., and Kuriyan, J. (2005) Structure of the autoinhibited kinase domain of CaMKII and SAXS analysis of the holoenzyme. *Cell* **123**, 849–860
80. Meador, W. E., Means, A. R., and Quiocho, F. A. (1993) Modulation of calmodulin plasticity in molecular recognition on the basis of X-ray structures. *Science* **262**, 1718–1721
81. Kanayama, A., Seth, R. B., Sun, L., Ea, C.-K., Hong, M., Shaito, A., *et al*. (2004) TAB2 and TAB3 activate the NF-κB pathway through binding to polyubiquitin chains. *Mol. Cell* **15**, 535–548
82. Xia, Z.-P., Sun, L., Chen, X., Pineda, G., Jiang, X., Adhikari, A., *et al*. (2009) Direct activation of protein kinases by unanchored polyubiquitin chains. *Nature* **461**, 114–119
83. Yang, W.-L., Wang, J., Chan, C.-H., Lee, S.-W., Campos, A. D., Lamothe, B., *et al*. (2009) The E3 ligase TRAF6 regulates akt ubiquitination and activation. *Science* **325**, 1134–1138
84. Filipčík, P., Curry, J. R., and Mace, P. D. (2017) When worlds collide—mechanisms at the interface between phosphorylation and ubiquitination. *J. Mol. Biol.* **429**, 1097–1113
85. Perez-Riverol, Y., Csordas, A., Bai, J., Bernal-Llinares, M., Hewapathirana, S., Kundu, D. J., *et al*. (2019) The PRIDE database and related tools and resources in 2019: improving support for quantification data. *Nucleic Acids Res.* **47**, D442–D450
86. Notredame, C., Higgins, D. G., and Heringa, J. (2000) T-coffee: a novel method for fast and accurate multiple sequence alignment 1 1Edited by J. Thornton. *J. Mol. Biol.* **302**, 205–217